Insight into the Neogene tectonic history of the northern Bolivian Orocline from new paleomagnetic and geochronologic data

Sonia Rousse, Stuart A. Gilder, Michel Fornari, Thierry Sempere

Insight into the Neogene tectonic history of the northern Bolivian Orocline from new paleomagnetic and geochronologic data

Sonia Rousse[1] and Stuart Gilder

Institut de Physique du Globe de Paris, Laboratoire de Paléomagnétisme, Paris, France

Michel Fornari

Institut de Recherche pour le Développement, UMR Géosciences Azur, Faculté des Sciences, Nice, France

Thierry Sempere

Institut de Recherche pour le Développement, Laboratoire Mécanismes de Transfert en Géologie, Institut des Sciences de la Terre, Toulouse, France

Received 25 October 2004; revised 22 April 2005; accepted 7 September 2005; published 22 November 2005.

[1] A paleomagnetic study of 36 sites (315 samples) of Neogene strata from the Peruvian Altiplano and adjacent sub-Andean belt (Pilcopata area), combined with $^{40}Ar/^{39}Ar$ dating of 13 lava flows, provide new constraints on the Cenozoic deformation history of the northern Bolivian Orocline. In the Peruvian Altiplano, $^{40}Ar/^{39}Ar$ dating brackets the age of the strata sampled for paleomagnetism between 26.5 and 12.1 Ma for the Huaccochullo basin, 18.6 and 12.1 Ma for the Descanso-Yauri basin, and 16.8 and 15.5 Ma for the Ayaviri basin. Sub-Andean sediments are paleontologically constrained as Miocene, yet pre-9 Ma. Prefolding magnetizations isolated in the Huaccochullo, Descanso-Yauri, and Pilcopata localities indicate significant counterclockwise vertical axis block rotations of 11.3° ± 5.4°, 31.0° ± 10.2° and 7.8° ± 4.8°, respectively. The pattern of rotations together with mapped structures suggest that deformation of the northern Altiplano was partitioned into large regions experiencing relatively minor rotation versus smaller, isolated basins exhibiting high-amplitude counterclockwise rotations that lie in a major left-lateral shear zone. Our new results imply significant transpressional deformation occurred throughout the Peruvian Altiplano since circa 12 Ma and are integrated in a model detailing the tectonic evolution of the northern Bolivian Orocline since 25 Ma. **Citation:** Rousse, S., S. Gilder, M. Fornari, and T. Sempere (2005), Insight into the Neogene tectonic history of the northern Bolivian Orocline from new paleomagnetic and geochronologic data, *Tectonics*, *24*, TC6007, doi:10.1029/2004TC001760.

1. Introduction

[2] The Andean Cordillera spans the entire Pacific margin of the South American continent, forming one of the Earth's longest and highest mountain belts. Between 15°S and 22°S, the orogen displays its greatest width (more than 700 km) (Figure 1), thickest crust (up to ~70 km) [*James*, 1971; *Wigger et al.*, 1994; *Beck et al.*, 1996; *Yuan et al.*, 2002], and the Earth's second largest high plateau, the Altiplano, with a mean elevation of ~3800 m. How and when this wide region of thick crust in the central Andes formed is hotly debated. Several workers have attributed crustal thickening mainly to horizontal tectonic shortening [*Lyon-Caen et al.*, 1985; *Isacks*, 1988; *Allmendinger et al.*, 1997; *Lamb et al.*, 1997; *McQuarrie*, 2002; *Müller et al.*, 2002; *Yang et al.*, 2003], despite the fact that most estimates of Neogene shortening amounts are too low to account for the entirety of the anomalously thick crust [*Kley and Monaldi*, 1998, and references therein; *Swenson et al.*, 2000; *Yuan et al.*, 2000; *Coutand et al.*, 2001; *McQuarrie and DeCelles*, 2001; *DeCelles and Horton*, 2003], leading some workers to invoke a component of pre-Neogene crustal thickening [*McQuarrie*, 2002; *Yang et al.*, 2003]. Others propose that magmatic addition and/or lateral ductile flow in the lower crust also participated in the crustal thickening [*James*, 1971; *Kono et al.*, 1989; *Wigger et al.*, 1994; *Schmitz et al.*, 1997; *James and Sacks*, 1999; *Springer*, 1999; *Yuan et al.*, 2000, 2002; *Brasse et al.*, 2002; *Babeyko et al.*, 2002; *Husson and Sempere*, 2003; *Yang et al.*, 2003; *Hindle et al.*, 2005]. Another topic of debate surrounds the timing of deformation that led to the build up of the plateau's present morphology. Some workers support a principally Late Cenozoic origin [*Isacks*, 1988; *Gubbels et al.*, 1993; *Jordan et al.*, 1997, 2001], others favor an Eocene age for the beginning of orogeny [*Kennan et al.*, 1995; *Lamb et al.*, 1997; *Viramonte et al.*, 1999; *DeCelles and Horton*, 2003], while *Sempere et al.* [1997] and *Horton et al.* [2001] have proposed ages as old as Late Cretaceous–early Paleocene.

[3] Not only is the region between 15°S and 22°S characterized by the world's second highest plateau, but within the same region, a progressive reorientation in

[1]Now at Geological Survey of Norway, Geodynamic Laboratory, Trondheim, Norway.

0278-7407/05/2004TC001760

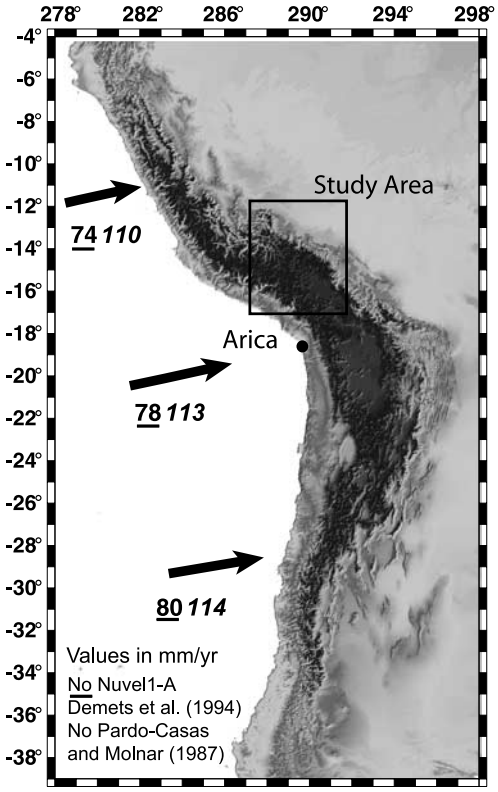

Figure 1. Topographic map of the Andean mountain range (>4000 m in black). Arrows represent convergence direction with rates indicated. Rectangle defines the area where paleomagnetic and $^{40}Ar/^{39}Ar$ samples were collected for this study.

geologic strike occurs that parallels the curved shape of the margin. The systematic change in strike of this large-scale structure, called the Bolivian Orocline, is also mimicked by a progressive change in the sense of paleomagnetic rotations, going from clockwise south of the bend to counterclockwise north of it (Figure 2) [*Randall*, 1998; *Beck*, 1998; *Roperch et al.*, 2000; *Lamb*, 2001; *Richards et al.*, 2004]. The origin and mechanism that caused such a pattern remain unclear; however, most workers agree that the tectonic evolution of the Bolivian Orocline can be better understood by mapping paleomagnetic rotations in space and time [*Beck*, 1988; *Isacks*, 1988; *Randall*, 1998; *Beck*, 1998; *Abels and Bishoff*, 1999; *Roperch et al.*, 2000; *Lamb*, 2001; *Somoza and Tomlinson*, 2002; *Yang et al.*, 2003; *Rousse et al.*, 2003; *Richards et al.*, 2004].

[4] Central to the way vertical axis paleomagnetic rotations can be used to constrain the tectonic history of the Andes is by knowing when they occurred and the size of the block that was rotated. As the length scale depends on fault density and geometry, interpreting the paleomagnetic rotations depends either on knowing the detailed local structural geology or by sampling dense enough that one can define the size of the rotated block. For the Bolivian Orocline, proposed kinematic block models of deformation range from large-scale oroclinal bending, with wholesale rotation of the two limbs [*Isacks*, 1988] to a series of smaller-scale block models [*Beck*, 1988; *Isacks*, 1988; *Aubry et al.*, 1996; *Randall et al.*, 1996, 2001; *Somoza et al.*, 1996; *Abels and Bishoff*, 1999; *Kley*, 1999; *Roperch et al.*, 2000; *Lamb*, 2001; *Somoza and Tomlinson*, 2002; *Richards et al.*, 2004]. Recently, *Riller and Oncken* [2003] proposed an alternative to the rigid block rotation model by arguing that paleomagnetic rotations are linked to shear on individual faults, with rotation sense and magnitude depending on the geometry of the fault with respect to the horizontal shear component acting in a transpressive shortening regime.

[5] Besides *Riller and Oncken* [2003], recent tectonic models of the Bolivian Orocline mostly invoke the existence of broad regions that experienced homogeneous rotations, bounded by narrow regions that facilitated enhanced deformation with rotations of local origin, uncorrelated to the broad regions around them [*Kley*, 1999; *Roperch et al.*, 2000; *Lamb*, 2001]. Although these models make predictions about how the northern (Peruvian) part of the Bolivian Orocline deformed in time and space, this region is completely void of relevant paleomagnetic data for the period when most workers agree that deformation was most active, e.g., since ~25 Ma (Figure 2). Indeed, only two studies report Cenozoic paleomagnetic poles for the entire Peruvian Altiplano. The first concerns the ~55 Ma Laguna Umayo locality (15.8°S, 289.9°E) which records a mean counterclockwise rotation of 32° ± 9° [*Butler et al.*, 1995; *Sigé et al.*, 2004; *Richards et al.*, 2004]. The second Cenozoic paleomagnetic pole is based on a mean of five sites of volcanic rocks located near Lake Titicaca [*Tsunakawa et al.*, 1987], for which K-Ar ages of 5–6 Ma are reported [*Kaneoka and Guevara*, 1984]. Unfortunately, five sites of volcanic rocks will not average geomagnetic secular variation, which renders this result useless for tectonic interpretations.

[6] Of the existing block models that concern the Peruvian part of the Bolivian Orocline, some of those testable by paleomagnetism are shown in Figure 3. *Roperch et al.* [2000] suggested that the forearc first deformed during the Late Cretaceous to Eocene, then deformation propagated to the regions farther east in the Miocene (Figure 3a). *Kley* [1999] put forward a structurally detailed model (Figure 3b), which divided the Bolivian Orocline into succinct structural domains, assigning each domain a sense and magnitude of rotation. *Kley* [1999] predicted that a large region encompassing the Peruvian Altiplano underwent an 8° counterclockwise rotation, with smaller blocks east and north of the Peruvian Altiplano experiencing from ~10° counterclockwise rotations to no rotation at all. *Lamb* [2001] proposed a three-stage evolution of the Bolivian Orocline (Figure 3c). Following *Roperch et al.* [2000], *Lamb* [2001] assumed that deformation and rotation first occurred in the forearc from ~45 to ~25 Ma. Next, between ~25 and 10 Ma, the locus of shortening migrated east toward the Eastern Cordillera and possibly to the western margin of the sub-Andes. Counterclockwise rotations of 10°–20° were predicted in a hinge zone at the northern extremity of the Peruvian Altiplano, with counterclockwise rotations of unknown magnitude occurring

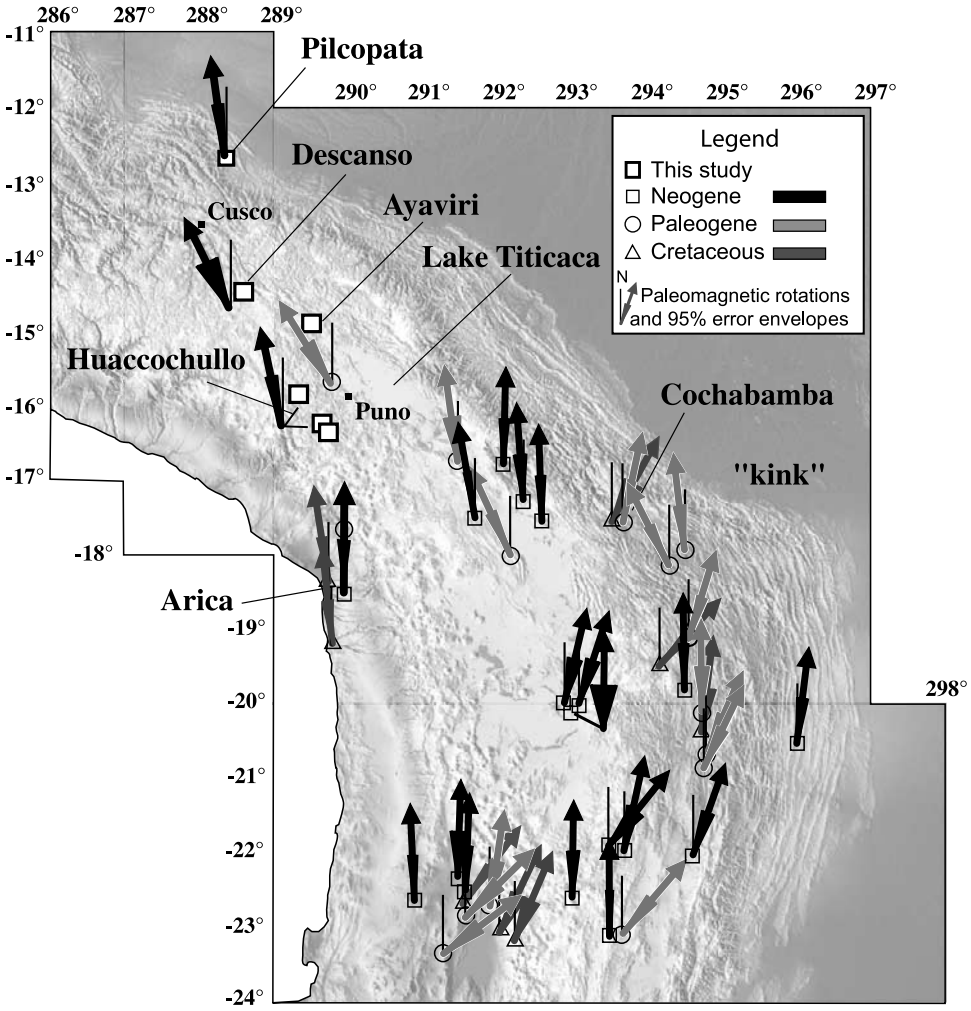

Figure 2. Paleomagnetic rotations in the central Andes. Data are from this study and compilations of *Rousse* [2002] and *Richards et al.* [2004]. All rotations have been recalculated using the reference poles from *Besse and Courtillot* [2002]. White squares indicate the sampling localities of the present study. The legend indicates the age of the strata and the corresponding paleomagnetic rotation (shown with 95% uncertainty envelop).

farther southeast (Figure 3c). Phase three occurred in the last 10 Myr, with up to 10° counterclockwise rotations occurring in the hinge zone of the Peruvian Altiplano, with larger vertical axis rotations associated within narrow shear zones. On the basis of Euler pole analysis of along strike variations in crustal shortening since 35 Ma (Figure 3d), *Richards et al.* [2004] proposed that the Eastern Cordillera experienced a wholesale 8° counterclockwise rotation from 35 to 10 Ma, while the sub-Andean zone underwent a 6° counterclockwise rotation during the past 10 Myr.

[7] To better constrain the Neogene deformation history of the northern (Peruvian) part of the Bolivian Orocline, we combined $^{40}Ar/^{39}Ar$ radiometric dating with a paleomagnetic study of Miocene strata from the Peruvian Altiplano and adjacent areas (Figure 4), which were previously void of such data. Samples were collected in the Huaccochullo basin over a region spanning ~5000 km^2 west of Lake Titicaca and in the Ayaviri and Descanso-Yauri basins, which lie closer to the Eastern Cordillera. Paleomagnetic samples were also collected from the sub-Andean belt near Pilcopata (Figure 4).

2. Geological Setting, Paleomagnetic Sampling and Age Constraints

[8] The highlands of the Western and Eastern cordilleras bound the Altiplano. Whereas stringers and clusters of volcanic cones dominate the landscape of the Western Cordillera, the Eastern Cordillera apparently results from crustal shortening that started in the late Oligocene [*Sempere et al.*, 1990]. The Huaccochullo, Ayaviri, and Descanso-Yauri basins are located in the northwestern Altiplano (Figure 4), at altitudes >3900 m, hence over a thickened crust. Unlike the Bolivian Altiplano, where active and fossil sedimentary basins predominate, the Peruvian

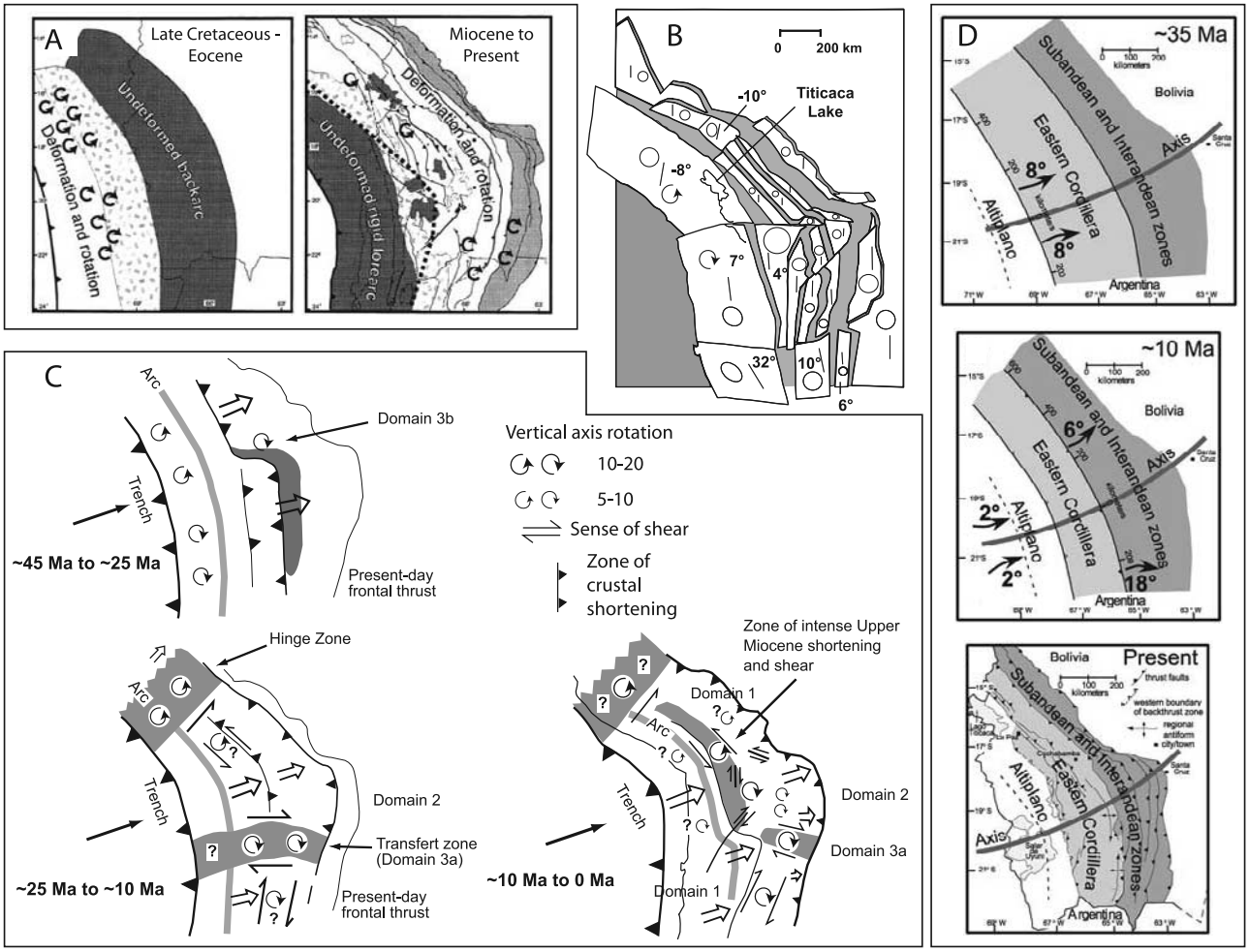

Figure 3. Recent kinematic models proposed for the tectonic evolution of the Bolivian Orocline from (a) *Roperch et al.* [2000]; (b) *Kley* [1999]; (c) *Lamb* [2001]; and (d) *Richards et al.* [2004].

Altiplano region is characterized by late Oligocene-Neogene basins and volcanic areas that are interspersed with uplifted belts of Paleozoic to Paleogene rocks.

[9] The overall fault pattern (Figure 4), the individual fault characteristics and the association of Cenozoic magmatism, including mantle-derived rocks, within the main fault systems, suggest that the upper crust of the northern Bolivian Orocline was deformed mainly by transpression, involving lithospheric-scale fault systems of subvertical geometry [*Sempere et al.*, 2002b]. Two first-order left-lateral transpressive fault systems occur in the highlands of southern Peru (Figure 4). One is the ~N130°E Urcos-Ayaviri-Copacabana-Coniri fault system (SFUACC in Spanish), which has a significant SW verging reverse component and played a major role in the development and syndepositional deformation of the sediments in the Ayaviri and Descanso-Yauri basins. The second is the seismically active ~N125°E trending Incapuquio fault system (SFI in Spanish), which has both large and small flower structures that have exhumed Precambrian basement. Reverse faults in this system mostly dip to the NE, with dips ranging from 85°–90° (dominant) to 35° [*Jacay et al.*, 2002; *Sempere et al.*, 2002a].

[10] Below, we discuss the geological context of the basins we sampled for paleomagnetism and $^{40}Ar/^{39}Ar$ dating. Details surrounding the $^{40}Ar/^{39}Ar$ and paleomagnetic results are given in sections 3 and 4, respectively. Paleomagnetic sampling sites are named P1XX (e.g., P143) while $^{40}Ar/^{39}Ar$ samples have identification numbers XXXXXX-X (e.g., 970815-1). A complete structural and stratigraphic analysis is beyond the scope of this paper. For further details the reader should refer to *Jacay and Sempere* [2004].

2.1. Huaccochullo Basin

[11] The Huaccochullo basin contains alluvial and lacustrine strata whose lithologies include mudstone, volcano-detritic sandstone, limestone with stromatolitic laminations, and minor conglomerate. In two distinct areas south and west of Puno (Figure 5a), we sampled volcano-detritic sandstone and limestone ascribed to the Pichu Formation. The lower part of the Pichu Formation contains basaltic flows that correlate laterally with the Tacaza Group basalts, dated between 30 and 25 Ma in this area [*Fornari et al.*,

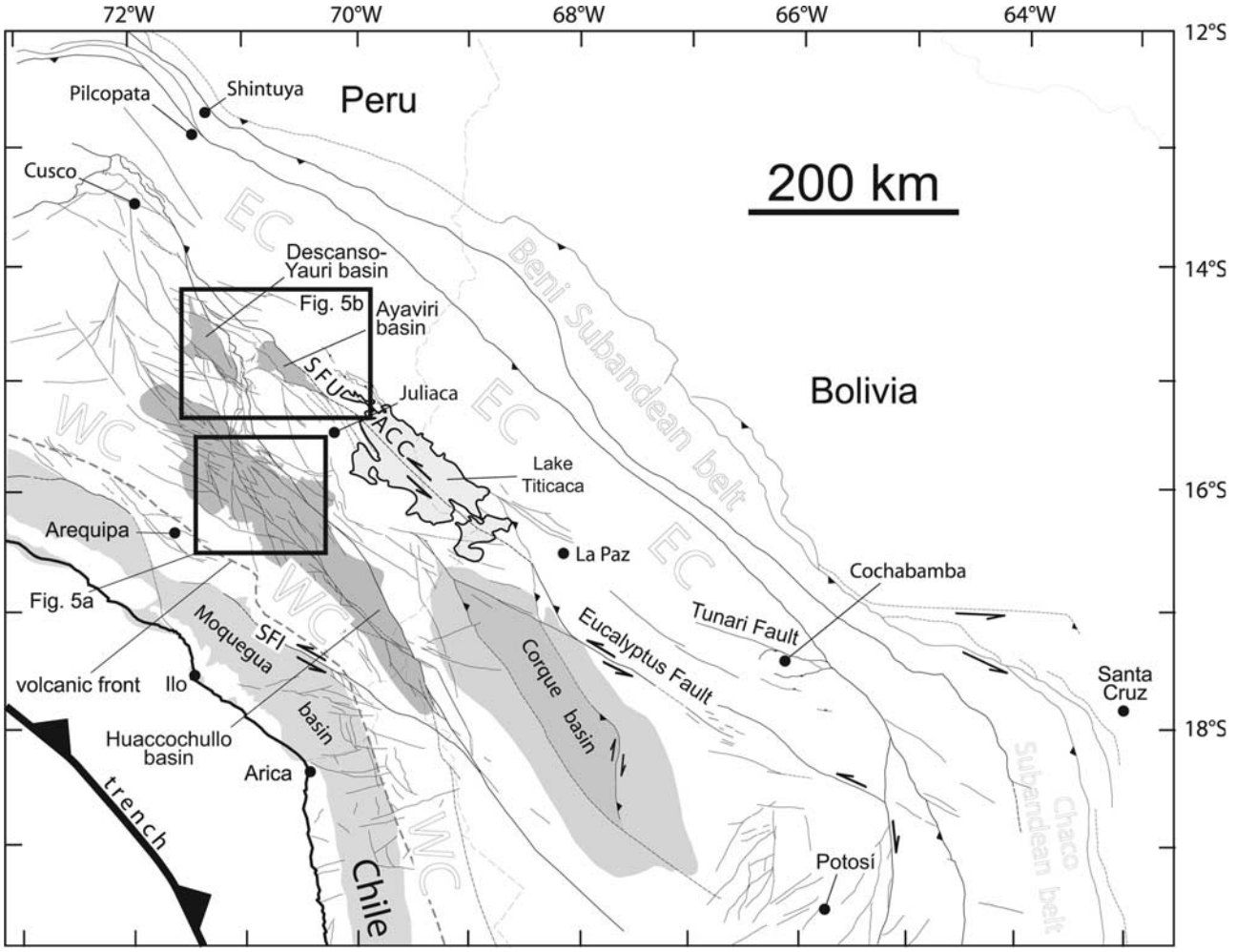

Figure 4. Simplified structural map of the northern Bolivian Orocline showing the major structural trends and the sedimentary basins discussed in the text.

2002]. The western area is located in the Río Ojecancha Valley (ROV, Figure 5a). There, paleomagnetic cores (sites P143–P145) were drilled in volcano-detritic sandstones that are located ~70 m above an 80 m thick basalt flow that yielded a 26.5 ± 0.1 Ma $^{40}Ar/^{39}Ar$ whole rock age (sample 970815-1, note that details surrounding the radiometric dating are discussed in the following section and $^{40}Ar/^{39}Ar$ data are given in Tables 1 and 2) and ~100 m below two tuffs dated at 24.5 ± 0.1 Ma and 24.1 ± 0.8 Ma (981005-1 and 981005-2). A local mean compacted sedimentation rate of ~85 m/Myr can thus be calculated for this part of the section, and an age of 25.7 ± 0.2 Ma (latest Oligocene) is estimated for the sampled strata.

[12] The southern sampling area actually comprises two subareas (PM and RJV, Figure 5a): one (paleomagnetic sites P129 through P134 and P138 through P140) is located on the road from Puno to Moquegua, ~4 km NE of the Huaccochullo Village, and the other (sites P141 and P142) lies in the neighboring Río Jatucachi Valley, ~11 km SE of the former. In both subareas, paleomagnetic cores were drilled within a ~490 m thick interval, above an ignimbrite that yielded $^{40}Ar/^{39}Ar$ dates of 13.5 ± 0.1 Ma on sanidine (011019-8 San) and 13.7 ± 0.2 on biotite (011019-8 biotite), and below a 40 m thick tuff that has a biotite $^{40}Ar/^{39}Ar$ date of 11.3 ± 0.4 Ma (011019-7). These dates bracket the sampled section within the 13.5 to 11.3 Ma interval, and yield a local mean compacted sedimentation rate of 223 m/Myr. Apart from volcanodetritic sandstone and limestone, we drilled one site (P139) consisting of a single andesite flow, sediments underlying the flow, and a whitish unwelded ashfall horizon immediately overlying the andesite. This site is located ~320 m above the 13.5 Ma ignimbrite and ~170 m below the 11.3 Ma tuff [*Cuéllar*, 2001], which, assuming a constant sedimentation rate, allows us to estimate its age at 12.1 Ma. Stratigraphic positions of our paleomagnetic sites relative to the dated volcanic units suggest that most of them, if not all, lie within the 13–12 Ma interval. The sampled strata are thus ~13 Myr younger than those sampled in the northwestern area of the same basin.

2.2. Ayaviri Basin

[13] The elongate Ayaviri basin is bounded by the Ayaviri and Pasani faults to its NE and SW, respectively (Figure 5b).

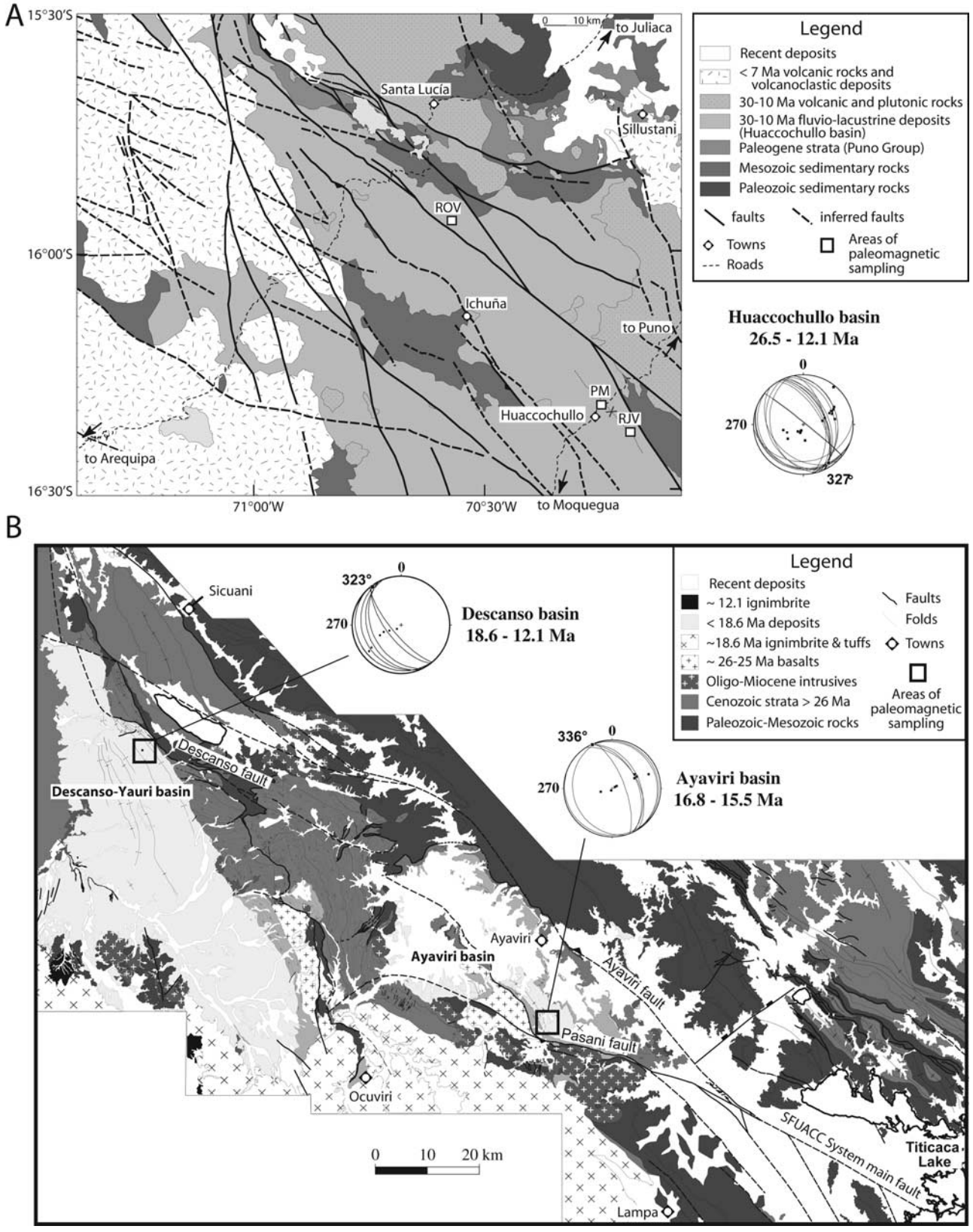
A
15°30'S
16°00'S
16°30'S
71°00'W
70°30'W
0 10 km
to Juliaca
Santa Lucía
Sillustani
ROV
Ichuña
to Puno
PM
Huaccochullo
RJV
to Arequipa
to Moquegua
Legend
Recent deposits
< 7 Ma volcanic rocks and volcanoclastic deposits
30-10 Ma volcanic and plutonic rocks
30-10 Ma fluvio-lacustrine deposits (Huaccochullo basin)
Paleogene strata (Puno Group)
Mesozoic sedimentary rocks
Paleozoic sedimentary rocks
faults
inferred faults
Towns
Roads
Areas of paleomagnetic sampling
Huaccochullo basin
26.5 - 12.1 Ma
0
270
327
B
Sicuani
323°
0
270
Descanso basin
18.6 - 12.1 Ma
Descanso fault
Descanso-Yauri basin
336°
0
270
Ayaviri basin
16.8 - 15.5 Ma
Ayaviri
Ayaviri basin
Ayaviri fault
Pasani fault
Ocuviri
SFUACC System main fault
Titicaca Lake
Lampa
0 10 20 km
Legend
Recent deposits
~ 12.1 ignimbrite
< 18.6 Ma deposits
~18.6 Ma ignimbrite & tuffs
~ 26-25 Ma basalts
Oligo-Miocene intrusives
Cenozoic strata > 26 Ma
Paleozoic-Mesozoic rocks
Faults
Folds
Towns
Areas of paleomagnetic sampling

Figure 5

Synsedimentary deformation (growth strata) related to the Ayaviri fault is older than ~25.2 Ma trachybasalt flows [*Fornari et al.*, 2002]. Growth strata along the Pasani fault are younger than a ~17.3 Ma ignimbrite (970822-3 and -4). Sediment accumulation clearly occurred during deformation along the faults bounding the basin [*Sempere et al.*, 2002a].

[14] We drilled 8 sites (69 samples) in well-lithified, conglomeratic sandstones, commonly with a red mudstone matrix, within the Tinajani Formation growth strata [*Rodríguez et al.*, 1999] near the SW boundary of the basin (Figure 5b). The sampled strata postdate a thick ignimbrite flow that yielded biotite $^{40}Ar/^{39}Ar$ dates of 17.5 ± 0.6 and 17.3 ± 0.1 Ma (970822-3 and -4) and are older than the Cerro Chignaya trachydacite neck, which we dated at 15.8 ± 0.8 Ma (990611-1). Strictly speaking, these ages bracket our sampled horizons between 17.3 ± 0.1 and 15.8 ± 0.8 Ma, i.e., to an interval spanning ~1.5 ± 0.9 Myr (a duration somewhere between 0.6 and 2.4 Myr, possibly closer to the short end-member as the Chignaya neck postdates the unit). The section above the 17.3 Ma ignimbrite is ~400 m thick [*Rodríguez et al.*, 1999], thus yielding a compacted accumulation rate estimated between 167 and 667 m/Myr, i.e., 450 ± 250 m/Myr on average. The oldest sampled strata (site P146) lie ~35 m above the 17.3 Ma ignimbrite, suggesting that their age is bracketed between 17.2 and 17.05 Ma. The youngest sampled strata (site P151) lie stratigraphically ~300 m above the 17.3 Ma ignimbrite, placing their age somewhere in the 16.8–15.5 Ma interval. The sampled section thus spans in time longer than 0.25 Myr but shorter than 1.7 Myr.

[15] Strata corresponding to sites P146–P151 clearly represent growth strata related to activity on the nearby Pasani fault. The dips of these beds decrease from to 69° to 42° (Table 3) within a stratigraphic thickness of ~130 m between sites P146 and P149; strata at the overlying sites P150, located ~555 m away from P149 in the dip direction, and stratigraphically ~120 m above, and P151, located ~550 m away from P150 in the dip direction, and stratigraphically ~50 m above, have dips of only 9° and 5°, respectively. This observation implies that the sediments were folded during or soon after deposition, and opens the possibility that their remanent magnetizations were acquired during or after folding.

2.3. Descanso-Yauri Basin

[16] The Descanso-Yauri basin (Figure 5b) is asymmetric in cross section [*Cerpa and Meza*, 2001; *Cerpa et al.*, 2004]. Its infill, the Descanso Formation, is much thicker (≥1000 m) in the NE than in the SW. The basin is bordered to its NE by the subvertical, NW striking Descanso fault that was clearly active during sedimentation, as attested by the presence of growth strata that consist of coarse conglomerates that are folded and even locally overturned. Along a section starting ~2 km SW of the Descanso fault, seven sites (61 samples) were drilled from the Descanso Formation red beds near the northeastern edge of the Descanso-Yauri basin (Figure 5b). Bedding dips at each site decrease with distance from the Descanso fault from 74° to 10° (Table 3). The red beds underlie the Yauri ashfall tuff, which yielded reliable sanidine $^{40}Ar/^{39}Ar$ dates of 12.1 ± 0.2 and 12.0 ± 0.3 Ma (970829-3). Below the red beds is a hydrothermally altered tuff, which *Boudesseul et al.* [2000] correlated with the Ocuviri ignimbrite. A sample of this tuff collected ~70 km SE of Descanso yielded $^{39}Ar/^{40}Ar$ biotite dates ranging from 18.7 ± 0.2 to 18.4 ± 0.1 Ma (mean age ~18.6 Ma; 970823-2, -3, -5). If the correlation is correct, the age of the sampled strata is bracketed between 18.6 and 12.1 Ma, albeit closer to 18.6 Ma due to stratigraphic proximity. The thickness of the stratigraphic portion bounded by the dated volcanic rocks is ~730 m [*Cerpa and Meza*, 2001], which yields a minimum mean compacted sedimentation rate of ~110 m/Myr.

[17] The lowest (oldest) paleomagnetic site, P154, lies ~50 m above the altered tuff and dips 65° to the SW; site P155 lies ~30 m above P154, with strata dipping 74° SW (the increase in dip is due to an anticlinal fold); site P156 is located ~850 m away from, and ~350 m above P155, with a ~40° SW dip; site P157 lies ~135 m away from, and ~50 m above P156, and dips 31° to the SW; sites P158 and P159 are located ~1400 m away from, and ~200 m above P157, with a 10° SW dip. It is clear that these sediments were folded during deposition, and as for the Ayaviri basin, this observation implies that the remanent magnetizations of the sediments were possibly acquired during or after folding.

2.4. Sub-Andean Belt at Pilcopata

[18] Farther east, beyond the northern Altiplano and the Eastern Cordillera, we collected paleomagnetic samples in the sub-Andean belt at ~600 m altitude along the road linking the town of Pilcopata to the village of Shintuya (Figure 4). There, the sub-Andean belt is a thin-skinned fold and thrust belt that probably initiated during the Upper Miocene [*Audebaud et al.*, 1973; *Noble and McKee*, 1977; *Jordan et al.*, 1997] and is seismically active today [*Jordan et al.*, 1983; *Dorbath et al.*, 1991]. Seven sites were drilled along the western flank of the NW striking Palotoa syncline in the Ipururo Formation, which is mainly composed of fine-grained sandstone. The Ipururo strata rest conformably on the Chambira Formation, inferred as Lower Oligocene in its lower part based on stratigraphic correlation and the presence of charophytes suggestive of the *Techtochara ucayaliensis* paleontological zone [*Vílchez and Romero*,

Figure 5. (a) Simplified structural map of the Huaccochullo basin with paleomagnetic sampling localities: ROV, Río Ojecancha Valley; PM, Puno-Moquegua road; RJV, Río Jatucachi Valley. (b) Simplified structural map of the area encompassing the Ayaviri and Descanso-Yauri basins. Paleomagnetic sampling localities, their age windows, and stereonet projections of bedding planes (lower hemisphere) and poles to bedding (upper hemisphere) are shown for the beds sampled for paleomagnetism. Both maps were modified after *Cerpa et al.* [2004], *Ibarra et al.* [2004], *Latorre et al.* [2004], *Mamani et al.* [2004], and *Rodríguez et al.* [1999].

Table 1. Summary of $^{40}Ar/^{39}Ar$ Age Data[a]

Sample	Rock Type	Location	Coordinates		DM	Weight, mg	Lab Number	Preferred Plateau Age		Steps	Isochron Age	Inverse correlation Diagram Ri	MSWD	Total Gas Age, Ma
			UTM-19 Easting	Northing				Age ± 2σ	^{39}Ar,%					
970815-1	augitic basalt lava flow	Rio Ojecancha	03 29 743	82 40 880	Wh R	2.90	V1380	26.50 ± 0.10	42 (MP)	8 of 16	26.21 ± 0.18[b]	353 ± 3	5.8	28.17 ± 0.10
981005-1	biotite rich welded tuff	Rio Ojecancha	03 25 573	82 34 184	biotite	0.26	V1367	24.48 ± 0.11	94	7 of 11	24.50 ± 0.15	282 ± 17	1.5	24.37 ± 0.14
981005-2	white-greenish tuff	Rio Ojecancha	03 24 974	82 32 522	biotite	0.13	V1648	24.09 ± 0.81	94	8 of 10	24.06 ± 0.60	295 ± 1	1.8	23.92 ± 0.78
011019-7	unwelded white tuff	Huaccochullo	03 65 983	81 93 340	biotite	0.28	G725	11.27 ± 0.35	76	7 of 11	11.86 ± 0.92	291 ± 2	3.2	10.80 ± 0.36
011019-8	ignimbritic flow	Huaccochullo	03 65 466	81 92 020	biotite	0.25	G728	13.70 ± 0.15	74	7 of 11	13.77 ± 0.46	288 ± 4	9.0	13.30 ± 0.16
011019-8	ignimbritic flow	Huaccochullo	03 65 466	81 92 020	San	0.45	G812	13.50 ± 0.06	95	4 of 6	13.49 ± 0.05	307 ± 18	0.34	13.53 ± 0.06
970822-3	tuff	Tinajani	03 30 853	83 42 127	biotite	0.11	V1646	17.54 ± 0.61	77	6 of 9	17.24 ± 3.00	300 ± 10	1.4	15.98 ± 0.58
970822-4	pumice rich tuff	Tinajani	03 30 853	83 42 127	biotite	0.31	V1553	17.25 ± 0.10	96	10 of 16	17.22 ± 0.29	296 ± 4	1.02	17.13 ± 0.12
990611-1	lava neck	Cerro Chignaya	03 47 300	83 35 460	Amph	0.27	G156	15.80 ± 0.75	94	3 of 7	15.26 ± 0.65	340 ± 55	0.25	15.99 ± 0.52
970823-2	ignimbritic flow	Buena Vista	02 92 490	83 39 570	biotite	0.26	V1462	18.74 ± 0.19	92	7 of 12	19.32 ± 0.29	278 ± 4	0.7	18.35 ± 0.32
970823-3	ignimbritic flow	Buena Vista	02 92 494	83 39 579	biotite	0.37	V1594	18.64 ± 0.13	88	12 of 19	18.31 ± 0.54	305 ± 8	0.7	18.26 ± 0.14
970823-5	ignimbritic flow	Buena Vista	02 92 494	83 39 579	biotite	0.19	V1645	18.38 ± 0.14	87	6 of 11	18.63 ± 0.30	284 ± 7	1.3	18.39 ± 0.16
970829-3	ashfall	Yauri	02 43 650	83 65 100	San	0.61	v1637	12.08 ± 0.18	95	5 of 9	12.18 ± 0.34	247 ± 54	2.6	11.90 ± 0.22
970829-3	ashfall	Yauri	02 43 650	83 65 100	San	0.26	v1638	11.99 ± 0.27	100	5 of 5	12.16 ± 0.34	263 ± 33	0.9	11.99 ± 0.27

[a]Lab number, laboratory experiment number; DM, dated material; Wh R, whole rock; San, sanidine; Amph, amphibole; Steps, number of temperature steps included in the plateau versus total number of steps; ^{39}Ar, percentage of total ^{39}Ar included in the plateau age; Ri = ($^{40}Ar/^{36}Ar$) initial ratio; MSWD, mean square of weighed deviation. Isochrons were fitted to all points except for sample 970815-1 (whole rock).
[b]First three steps excluded.

1998]. An angular unconformity (Ucayali unconformity) separates Ipururo strata from the overlying Quaternary Madre de Dios Formation. About 4 m above the Ucayali unconformity, $^{40}Ar/^{39}Ar$ dating on the ~1.5 m Cocama ash (10°24′55″S, 71°10′22″W) gave an age of 9.0 ± 0.3 Ma [*Campbell et al.*, 2001]. On the basis of these considerations, the Ipururo Formation is likely Miocene in age, being older than ~9 Ma but significantly younger than Lower Oligocene.

3. Radiometric $^{40}Ar/^{39}Ar$ Dating

3.1. Sample Preparation and Methodology

[19] Except for sample 970815-1, which is a whole rock fraction, analyses were performed on individual mineral grains (Table 1). To extract the mineral separates, samples were first crushed and sieved through mesh sizes of 800–500 and 500–300 μm. Minerals were then handpicked under a binocular microscope. Mineral concentrates were wrapped in aluminum foil and irradiated at McMaster University's (Hamilton, Canada) nuclear reactor (position 5C), with irradiation times of 5 hours, except for biotite samples 011019-7 and 011019-8, which were irradiated for 25 hours and for amphibole sample 990611-5 for 70 hours. Fish Canyon sanidine was used as a neutron flux monitor (J value determination) assuming an age of 28.02 Ma [*Renne et al.*, 1998]. Argon isotopic concentrations were measured at the UMR Géosciences Azur Geochronology Laboratory (University of Nice, France). Stepwise heating was performed with a 50 W Synrad CO_2 laser or a Coherent Innova 70-4 continuous Argon ion laser. Each step lasted three minutes, including one minute for heating and cleaning the gas, before introducing it into the spectrometer. Isotopes were measured statically with a VG3600 mass spectrometer using a Daly detector.

[20] Dates were calculated from the measured isotopic ratios corrected for mass discrimination, system blanks, and interfering isotopes produced during irradiation. Blanks for the extraction and purification system, routinely measured every three steps, were in the range of $40–90 \times 10^{-14}$, $2–10 \times 10^{-14}$ and $2–6 \times 10^{-14}$ cm^3 STP at masses 40, 39 and 36, respectively. Mass discrimination was monitored by regularly analyzing air pipette volumes. Uncertainty on the $^{40}Ar^*/^{39}Ar_K$ ratio of the monitor was estimated at 0.5% and was included in the uncertainty calculation of the plateau age (Table 1). The following criteria were used to determine plateau ages: (1) the plateau should contain at least 70% released ^{39}Ar, (2) the plateau should include at least three consecutive temperature steps, and (3) the integrated age of the plateau should concur within 2σ of each apparent age from the plateau.

3.2. Results

[21] The Ar data are given in Table 1 and the preferred dates corresponding to the plateau ages are illustrated in Figure 6. Inverse isochron ages, total gas ages and the plateau ages are concordant at the 2σ level for all the samples except for the whole rock sample (970815-1) (see

Table 2. The $^{40}Ar/^{39}Ar$ Analytical Data[a]

Step	Laser Power, mW	Atmospheric Contamination,%	^{39}Ar (%)	$^{37}Ar_{Ca}/^{39}Ar_K$	$^{40}Ar^*/^{39}Ar_K$	Age, Ma ± 1σ
V1380: Sample 970815-1, Whole Rock, 2.90 mg, MC23 (5 hours), J = 0.001204275						
1	60	96.88	0.2	1.410	22.43	48.10 ± 10.87
2	110	89.98	0.32	1.408	38.88	82.57 ± 5.78
3	180	83.13	0.57	1.390	29.52	63.03 ± 2.51
4	280	62.18	2.91	0.989	17.03	36.63 ± 0.45
5	380	50.45	7.14	0.844	15.00	32.31 ± 0.25
6	480	36.71	16.10	0.594	13.82	29.78 ± 0.14
7	525	11.58	8.44	0.411	12.58	27.14 ± 0.11
8	570	6.16	7.88	0.381	12.40	26.75 ± 0.08
9	620	4.65	6.64	0.373	12.39	26.72 ± 0.11
10	710	5.09	6.88	0.392	12.29	26.51 ± 0.10
11	820	4.75	8.02	0.388	12.29	26.50 ± 0.10
12	950	4.77	6.71	0.432	12.28	26.49 ± 0.11
13	1100	5.54	1.81	0.821	12.17	26.26 ± 0.22
14	1400	4.84	1.37	2.013	12.28	26.48 ± 0.43
15	2050	3.45	2.64	2.271	12.13	26.17 ± 0.16
Fuse	5500	3.97	22.37	4.719	12.11	26.12 ± 0.06
						28.17 ± 0.05[b]
V1367: Sample 981005-1, Biotite, 0.26 mg, MC23 (5 hours), J = 0.001204275						
1	70	87.11	0.27	0.091	6.97	15.09 ± 8.61
2	145	95.71	0.34	0.000	1.25	2.72 ± 11.67
3	240	50.97	1.19	0.040	10.05	21.71 ± 1.78
4	360	11.62	4.23	0.010	11.61	25.05 ± 0.33
5	480	6.60	9.29	0.014	11.30	24.40 ± 0.16
6	580	3.96	18.72	0.015	11.39	24.57 ± 0.09
7	680	2.86	20.15	0.023	11.28	24.34 ± 0.09
8	780	2.25	20.70	0.030	11.30	24.39 ± 0.11
9	890	1.03	14.66	0.083	11.39	24.57 ± 0.12
10	1150	0.85	8.16	0.089	11.43	24.67 ± 0.27
Fuse	5500	2.74	2.29	0.064	11.56	24.95 ± 0.82
						24.37 ± 0.07[b]
V1648: Sample 981005-2, Biotite, 0.13 mg, MC23 (5 hours), J = 0.001204275						
1	65	89.01	1.71	0.000	9.31	20.11 ± 2.99
2	130	85.76	4.60	0.000	10.06	21.72 ± 1.63
3	210	84.05	5.79	0.000	10.74	23.19 ± 1.56
4	310	81.18	5.41	0.000	11.10	23.97 ± 1.41
5	460	78.64	10.46	0.000	11.43	24.66 ± 1.10
6	640	83.86	17.00	0.000	10.81	23.35 ± 1.38
7	820	77.18	23.40	0.000	11.42	24.65 ± 1.01
8	1000	54.50	13.38	0.000	11.34	24.48 ± 0.45
9	1200	16.99	10.53	0.000	11.01	23.76 ± 0.28
Fuse	5500	8.57	7.73	0.000	11.03	23.82 ± 0.44
						23.92 ± 0.39[b]
G725: Sample 011019-7, Biotite, 0.28 mg, MC35 (25 hours), J = 0.005930141						
1	425	98.30	1.64	0.031	0.84	8.93 ± 3.65
2	550	93.37	10.04	0.019	0.81	8.63 ± 0.88
3	630	88.42	10.52	0.019	0.91	9.72 ± 0.58
4	720	83.31	9.77	0.019	1.01	10.79 ± 0.42
5	835	80.35	6.60	0.020	1.02	10.82 ± 0.58
6	940	81.74	6.17	0.026	1.01	10.76 ± 0.39
7	1055	82.48	9.36	0.031	1.02	10.90 ± 0.50
8	1215	81.56	13.81	0.031	1.05	11.20 ± 0.43
9	1420	80.58	26.01	0.046	1.10	11.78 ± 0.34
10	1570	78.15	4.17	0.206	1.11	11.85 ± 0.46
Fuse	2500	66.36	1.91	0.694	1.13	12.02 ± 0.95
						10.82. ± 0.18[b]
G728: Sample 011019-8, Biotite, 0.25 mg, MC35 (25 hours), J = 0.005930141						
1	450	97.84	1.30	0.014	0.81	8.59 ± 2.73
2	560	89.41	3.28	0.009	0.72	7.68 ± 0.79
3	660	65.44	5.57	0.008	1.12	11.92 ± 0.38
4	785	48.31	8.53	0.007	1.25	13.31 ± 0.21
5	900	38.42	9.69	0.006	1.27	13.50 ± 0.20
6	1050	31.81	16.23	0.004	1.30	13.79 ± 0.14
7	1200	36.50	17.18	0.005	1.29	13.73 ± 0.18
8	1350	45.63	18.84	0.006	1.30	13.83 ± 0.21

Table 2. (continued)

Step	Laser Power, mW	Atmospheric Contamination,%	^{39}Ar (%)	$^{37}Ar_{Ca}/^{39}Ar_K$	$^{40}Ar^*/^{39}Ar_K$	Age, Ma ± 1σ
9	1500	39.68	12.53	0.005	1.30	13.90 ± 0.14
10	1755	22.35	4.34	0.002	1.25	13.28 ± 0.37
Fuse	2600	31.45	2.52	0.002	1.14	12.13 ± 0.51
						13.30. ± 0.08[b]
		G812: Sample 011019-8, Sanidine, 0.45 mg, MC35 (25 hours), J = 0.005930141				
1	400	52.36	0.82	0.014	1.34	14.24 ± 1.20
2	490	5.29	4.24	0.009	1.30	13.86 ± 0.23
3	550	6.26	6.69	0.012	1.26	13.44 ± 0.15
4	615	3.55	36.84	0.012	1.27	13.48 ± 0.04
5	710	1.26	6.68	0.011	1.27	13.58 ± 0.18
Fuse	2000	1.66	44.73	0.012	1.27	13.53 ± 0.03
						13.53. ± 0.03[b]
		V1646: Sample 970822-3, Biotite, 0.11 mg, MC23 (5 hours), J = 0.00120427479				
1	70	96.89	4.07	2.076	3.71	8.04 ± 3.11
2	125	91.59	6.26	1.038	3.60	7.80 ± 1.17
3	200	81.78	12.55	3.746	6.02	13.03 ± 0.73
4	300	75.41	13.40	0.000	7.44	16.10 ± 0.75
5	430	71.72	13.82	0.000	7.82	16.92 ± 0.72
6	600	72.12	21.59	0.000	8.44	18.24 ± 0.59
7	780	71.69	17.62	0.260	8.33	18.02 ± 0.66
8	1050	62.45	6.77	0.000	8.35	18.06 ± 0.78
Fuse	5500	51.78	3.92	0.000	8.26	17.85 ± 1.21
						15.98 ± 0.29[b]
		V1553: Sample 970822-4, Biotite, 0.31 mg, MC23 (5 hours), J = 0.00121079445				
1	55	99.87	0.05	0.001	1.471	3.21 ± 29.97
2	110	89.08	0.11	0.000	13.633	29.54 ± 10.92
3	180	71.14	0.18	3.540	8.38	18.22 ± 8.99
4	275	35.33	0.83	0.000	8.231	17.90 ± 1.41
5	355	17.69	1.93	0.000	7.807	16.98 ± 0.56
6	455	11.27	4.99	0.000	7.969	17.33 ± 0.24
7	585	5.36	7.52	0.027	8.022	17.44 ± 0.21
8	690	4.79	9.56	0.023	8.021	17.44 ± 0.16
9	780	3.59	11.41	0.030	7.963	17.31 ± 0.14
10	880	3.63	16.48	0.013	7.942	17.27 ± 0.12
11	980	2.57	13.85	0.000	7.964	17.32 ± 0.12
12	1090	4.15	6.68	0.217	7.758	16.87 ± 0.20
13	1300	1.76	16.45	0.179	7.928	17.24 ± 0.09
14	1460	4.59	5.78	0.101	7.703	16.75 ± 0.21
15	1800	2.11	3.09	0.321	7.926	17.23 ± 0.41
Fuse	5500	21.58	1.09	0.051	6.545	14.24 ± 0.87
						17.13 ± 0.06[b]
		G156: Sample 990611-1, Amphibole, 0.27 mg, MC26 (70 hours), J = 0.0175314359				
1	300	100.00	0.04	37.214	-	-
2	440	75.93	0.11	8.323	1.945	60.47 ± 150.96
3	620	49.82	1.35	4.829	0.556	17.48 ± 10.41
4	700	5.89	3.71	4.934	0.618	19.43 ± 3.08
5	820	8.35	55.53	4.932	0.503	15.84 ± 0.45
6	930	4.83	25.48	4.920	0.504	15.86 ± 0.83
Fuse	2200	9.86	13.79	4.900	0.493	15.52 ± 1.02
						15.99 ± 0.46[b]
		V1462: Sample 970823-2, Biotite, 0.26 mg, MC23 (5 hours), J = 0.00121361025				
1	80	96.99	0.11	0.076	6.10	13.32 ± 33.11
2	150	96.56	0.73	0.053	3.57	7.79 ± 5.83
3	250	86.77	2.19	0.027	5.06	11.04 ± 2.59
4	288	91.65	0.14	0.275	2.69	5.88 ± 30.95
5	345	52.41	3.51	0.000	8.51	18.53 ± 0.68
6	450	47.53	5.51	0.000	8.40	18.30 ± 0.43
7	650	41.97	11.76	0.002	8.49	18.50 ± 0.29
8	870	33.12	30.67	0.010	8.64	18.82 ± 0.16
9	1050	28.65	20.70	0.014	8.69	18.93 ± 0.18
10	1300	27.89	12.84	0.107	8.62	18.77 ± 0.21
11	1700	24.37	7.62	0.081	8.60	18.73 ± 0.35
Fuse	5500	37.90	4.22	0.175	7.20	15.70 ± 2.21
						18.35 ± 0.16[b]

Table 2. (continued)

Step	Laser Power, mW	Atmospheric Contamination,%	^{39}Ar (%)	$^{37}Ar_{Ca}/^{39}Ar_K$	$^{40}Ar^*/^{39}Ar_K$	Age, Ma ± 1σ
V1594: Sample 970823-3, Biotite, 0.37 mg, MC23 (5 hours), J = 0.00121361025						
1	70	97.06	0.18	0.804	5.80	12.66 ± 7.12
2	120	96.16	0.30	0.679	3.78	8.27 ± 4.83
3	190	91.66	0.65	0.000	4.85	10.59 ± 4.21
4	320	85.80	2.02	0.356	5.41	11.80 ± 0.83
5	390	69.51	1.84	0.334	7.08	15.44 ± 0.63
6	500	61.06	2.90	0.036	7.52	16.39 ± 0.40
7	600	49.16	3.95	0.000	8.25	17.98 ± 0.37
8	710	42.30	5.76	0.000	8.65	18.84 ± 0.29
9	810	38.44	5.70	0.000	8.49	18.49 ± 0.28
10	915	34.25	9.48	0.156	8.53	18.58 ± 0.18
11	1000	32.39	7.39	0.241	8.61	18.75 ± 0.18
12	1105	31.99	6.01	0.371	8.55	18.63 ± 0.20
13	1220	33.72	6.91	0.013	8.56	18.65 ± 0.24
14	1350	33.72	11.59	0.087	8.59	18.72 ± 0.17
15	1475	31.58	13.83	0.103	8.62	18.78 ± 0.14
16	1610	30.13	6.89	0.000	8.43	18.36 ± 0.25
17	1800	27.58	3.82	0.000	8.41	18.32 ± 0.30
18	2070	22.51	4.11	0.000	8.69	18.93 ± 0.34
Fuse	5500	21.61	6.67	0.025	8.43	18.37 ± 0.24
						18.26 ± 0.07[b]
V1645: Sample 970823-5, Biotite, 0.19 mg, MC23 (5 hours), J = 0.0012042748						
1	50	97.33	0.36	0.001	2.752	6.03 ± 5.79
2	130	79.62	1.98	0.000	5.327	11.66 ± 0.90
3	230	43.57	6.11	0.000	8.171	17.86 ± 0.30
4	320	28.15	8.15	0.000	8.646	18.89 ± 0.27
5	420	22.10	13.64	0.000	8.532	18.65 ± 0.18
6	520	16.43	14.75	0.000	8.443	18.45 ± 0.19
7	620	13.42	15.97	0.000	8.518	18.61 ± 0.13
8	720	12.13	15.48	0.000	8.484	18.54 ± 0.15
9	900	11.10	19.03	0.000	8.473	18.52 ± 0.12
10	1130	9.66	3.70	1.248	8.823	19.28 ± 0.52
Fuse	5500	32.66	0.81	0.000	8.635	18.87 ± 2.49
						18.39 ± 0.07[b]
V1637: Sample 970829-3, Sanidine, 0.61 mg, MC23 (5 hours), J = 0.0011923513						
1	170	100.00	0.12	0.004	-	-
2	250	100.00	0.12	0.004	-	-
3	360	68.47	0.52	0.001	6.07	13.01 ± 6.50
4	560	34.56	4.67	2.290	4.08	8.75 ± 0.87
5	770	12.39	8.32	0.421	5.47	11.73 ± 0.48
6	1030	14.13	6.99	0.000	5.37	11.52 ± 0.34
7	1300	4.68	4.69	0.000	6.03	12.93 ± 0.50
8	1900	10.28	6.42	0.000	5.61	12.02 ± 0.64
Fuse	5500	4.31	68.14	0.747	5.66	12.13 ± 0.08
						11.90 ± 0.11[b]
V1638: Sample 970829-3, Sanidine, 0.26 mg, MC23 (5 hours), J = 0.0011923513						
1	150	26.04	16.44	0.251	5.44	11.79 ± 0.40
2	240	5.54	22.55	0.451	5.71	12.37 ± 0.25
3	360	8.51	17.63	0.104	5.40	11.69 ± 0.35
4	600	6.28	7.67	0.000	5.69	12.33 ± 0.71
Fuse	5500	5.08	35.71	1.029	5.66	12.27 ± 0.18
						11.99 ± 0.14[b]

[a]Here ^{39}Ar (%) is fraction of ^{39}Ar released for each step; $^{37}Ar_{Ca}/^{39}Ar_K$ is Ar isotopes produced by Ca and K neutron interferences; $^{40}Ar^*$ is radiogenic ^{40}Ar. Error bars are at the 1σ level and do not include the error of the J irradiation parameter. Correction factors for the interfering isotopes produced by nuclear reactions on potassium and calcium in the McMaster reactor were $(^{39}Ar/^{37}Ar)_{Ca} = 7.06 \times 10^{-4}$ (±4%), $(^{36}Ar/^{37}Ar)_{Ca} = 2.79 \times 10^{-4}$ (±3%) and $(^{40}Ar/^{39}Ar)_K = 2.79 \times 10^{-2}$ (±4%). Isotopic ratios were corrected for blank and mass discrimination (1.00721 ± 0.19%). Ages were calculated using the decay constants proposed by *Steiger and Jager* [1978]. Steps in bold were used for the plateau age calculation.

[b]Total gas age.

Table 2 for analytical data). All laser heating experiments yielded reliable age data, yet some samples require a few additional comments. For example, the whole rock sample 970815-1 displays decreasing apparent ages versus temperature (Figure 6), likely indicating that some ^{39}Ar recoil affected the sample during irradiation. Only a mini plateau accounting for 42% of the total degassed ^{39}Ar is used as the best estimated age for this sample, which discards the high-

Table 3. High-Temperature/High-Coercivity Paleomagnetic Results From the Altiplano Basins (14°S–17°S) and the Pilcopata Region of the Sub-Andean Belt[a]

Site	λs, °S	ϕs, °W	Average Strike/Dip	no/No	N/R	Geographic				Stratigraphic			
						D_g	I_g	k	α_{95}	D_s	I_s	k	α_{95}
Huaccochullo Basin													
P129	16°16.43′	70°10.59′	84.3/26.5	8/9	0/4	167.0	60.6	48.9	8.4	170.0	34.2	48.9	8.4
P130	16°23.50′	70°18.92′	154.0/29.7	9/10	4/2	350.3	−31.6	61.6	6.8	3.8	−19.7	61.6	6.8
P131	16°23.40′	70°18.52′	155.8/34.7	6/9	1/5	148.7	20.3	33.8	11.7	159.9	15.5	32.8	11.9
P132	16°20.87′	70°15.52′	346.6/33.7	7/8	7/0	5.3	−21.4	144.6	5.0	349.6	−28.0	154.1	4.9
P133	16°20.61′	70°15.55′	336.4/51.1	6/8	6/0	2.3	−21.9	25.6	13.5	335.5	−34.0	28.1	12.9
P134	16°20.57′	70°15.56′	342.5/51.0	8/10	0/3	194.8	−1.3	46.6	8.7	185.8	23.8	55.2	8.0
P138	16°20.57′	70°15.56′	334.3/52.0	10/10	5/2	11.7	−13.3	39.2	7.9	347.6	−37.4	39.2	7.9
P139[b]	16°20.47′	70°15.48′	333.0/57.0	10/11	0/7	193.4	−25.1	324.4	2.7	197.4	15.1	324.4	2.7
P140	16°20.47′	70°15.48′	330.2/60.7	8/9	3/2	351.4	−7.4	25.3	11.5	334.1	−22.1	25.3	11.5
P141	16°25.28′	70°10.88′	309.0/87.2	9/10	3/3	158.2	−23.5	25.0	10.7	156.7	25.3	25.0	10.7
P142	16°25.28′	70°10.88′	306.5/82.0	8/9	1/4	159.4	−17.8	31.2	10.4	151.6	28.0	31.2	10.4
P143	15°55.68′	70°35.78′	111.3/14.3	10/10	7/0	339.5	−33.0	56.1	6.6	344.3	−21.9	56.1	6.6
P144	15°55.68′	70°35.78′	129.2/14.7	9/10	5/0	354.5	−37.5	69.6	6.4	0.6	−26.5	69.6	6.4
P145	15°56.31′	70°35.69′	111.9/11	8/9	8/0	341.2	−21.6	119.9	5.1	343.4	−13.2	138.2	4.7
Mean				13/14		171.5	18.0	9.8	14.0	166.4	25.8	42.2	6.5
Ayaviri Basin													
P146[c]	15°02.17′	70°35.10′	339.8/69	3/8	2/1	3.5	−34.2	62.9	15.7	310.8	−31.5	62.9	15.7
P147	15°02.10′	70°35.03′	327.7/45.8	9/9	4/0	352.6	−22.1	18.8	12.7	327.8	−32.8	18.8	12.7
P148	15°02.10′	70°35.03′	334.1/46.7	7/8	4/0	343.5	−13.3	35.1	10.8	330.7	−15.8	35.1	10.8
P149	15°02.10′	70°35.03′	335.4/42.0	9/9	5/0	335.5	−8.8	43.8	8.0	329.6	−6.6	43.8	8.0
P150[b]	15°01.58′	70°34.92′	331.9/8.8	8/9	5/0	341.1	−28.3	9.3	19.6	336.4	−29.3	9.3	19.6
P151	15°01.22′	70°34.75′	332.3/5.0	7/8	7/0	353.2	−27.5	21.6	13.3	350.7	−29.2	21.6	13.3
P152	15°00.17′	70°34.56′	162.4/20	9/9	9/0	4.2	−25.9	31.7	9.3	11.4	−17.4	31.7	9.3
P153	15°00.25′	70°34.74′	117.3/4.0	8/9	8/0	2.8	−22.6	36.9	9.2	3.4	−19.0	36.9	9.2
Mean				7/8		353.2	−22.4	36.7	10.1	341.0	−23.0	13.5	17.1
Descanso-Yauri Basin													
P154[b]	14°30.86′	71°18.70′	142.5/65.0	3/8	1/2	99.4	7.0	69.8	14.9	128.8	41.8	69.8	14.9
P155	14°30.86′	71°18.70′	140.2/74.0	9/9	0/9	108.7	22.6	36.5	8.6	157.1	34.8	36.5	8.6
P156	14°31.89′	71°18.65′	153.6/39.8	7/9	7/0	345.3	−20.0	157.4	4.8	355.3	−7.8	157.4	4.8
P157[b]	14°32.09′	71°18.67′	157.8/31.4	6/9	0/6	30.2	−25.8	11.1	21.0	34.5	0.0	11.1	21.0
P158	14°32.26′	71°19.44′	135.6/9.5	10/10	10/0	333.1	−34.0	72.8	5.7	338.8	−30.7	72.8	5.7
P159	14°32.26′	71°19.44′	135.3/9.5	8/8	8/0	323.7	−29.2	23.5	11.7	328.7	−27.4	23.5	11.7
P160	14°39.43′	71°15.93′	153.4/21.5	6/8	3/0	310.3	−17.2	178.1	5.4	318.1	−24.3	178.1	5.4
Mean				6/7		132.7	23.4	10.1	22.1	152.0	28.7	19.4	15.6
Mean				5/7		125.9	23.3	12.2	22.8	146.6	32.3	42.0	11.9
Sub-Andean Belt at Pilcopata													
P161	12°39.88′	71°20.45′	141.3/44.5	8/9	8/0	310.2	−41.5	57.9	7.3	342.9	−37.4	57.9	7.3
P162	12°39.97′	71°20.78′	122.5/27.0	8/8	0/8	153.9	30.2	39.4	8.9	163.0	14.1	39.4	8.9
P163	12°40.38′	71°20.75′	134.5/32.0	5/8	5/0	347.4	−41.4	38.0	12.6	2.3	−20.2	38.0	12.6
P164	12°40.70′	71°20.71′	125.5/19.0	9/9	0/9	157.5	30.6	52.3	7.2	164.8	19.4	52.3	7.2
P165	12°41.42′	71°20.97′	115.6/8.0	5/8	0/5	163.8	32.7	68.0	9.3	166.8	26.6	68.0	9.3
P166	12°41.99′	71°20.24′	78.6/4.0	7/8	0/7	168.0	31.0	33.0	10.7	168.0	27.0	33.0	10.7
P167	12°42.71′	71°21.74′	46.6/9.0	9/9	0/6	174.7	24.1	39.5	8.5	172.7	16.9	39.5	8.5
Mean				7/7		160.0	33.8	36.8	10.1	169.3	22.9	74.5	7.0

[a]Parameters are λs, site latitude; ϕs, site longitude; no/No, number of samples retained in the mean/total number of samples demagnetized; N, R, of the retained samples, number possessing normal (N) or reversed (R) polarity (note that no polarity was assigned to samples whose directions were determined with great circles); D, declination; I, inclination; k, best estimate of the precision parameter; α_{95}, radius of the cone in which the mean direction lies within 95% confidence.

[b]Site rejected.

[c]Site partly remagnetized due to lightening (see text).

temperature steps corresponding to the degassing of low-K mineral phases as indicated by the increase in $^{37}Ar_{Ca}/^{39}Ar_K$. Recoil clearly affects the correlation between $^{36}Ar/^{40}Ar$ and $^{39}Ar/^{40}Ar$, and the mean age calculated from all temperature steps produces a very large MSWD of 55. If one excludes the older apparent ages, the isochron age remains roughly the same (26.2 ± 0.2 Ma). The MSWD is reduced to 5.8, but the data remain scattered. In addition, both the isochron age and the $^{40}Ar/^{36}Ar$ intercept are poorly constrained. Therefore the age determined from this sample should be regarded with caution.

[22] Biotite spectra of samples 981005-2, 011019-8, 011019-7, 970822-3, and 970823-3 show progressively increasing apparent ages at low temperatures before flatten-

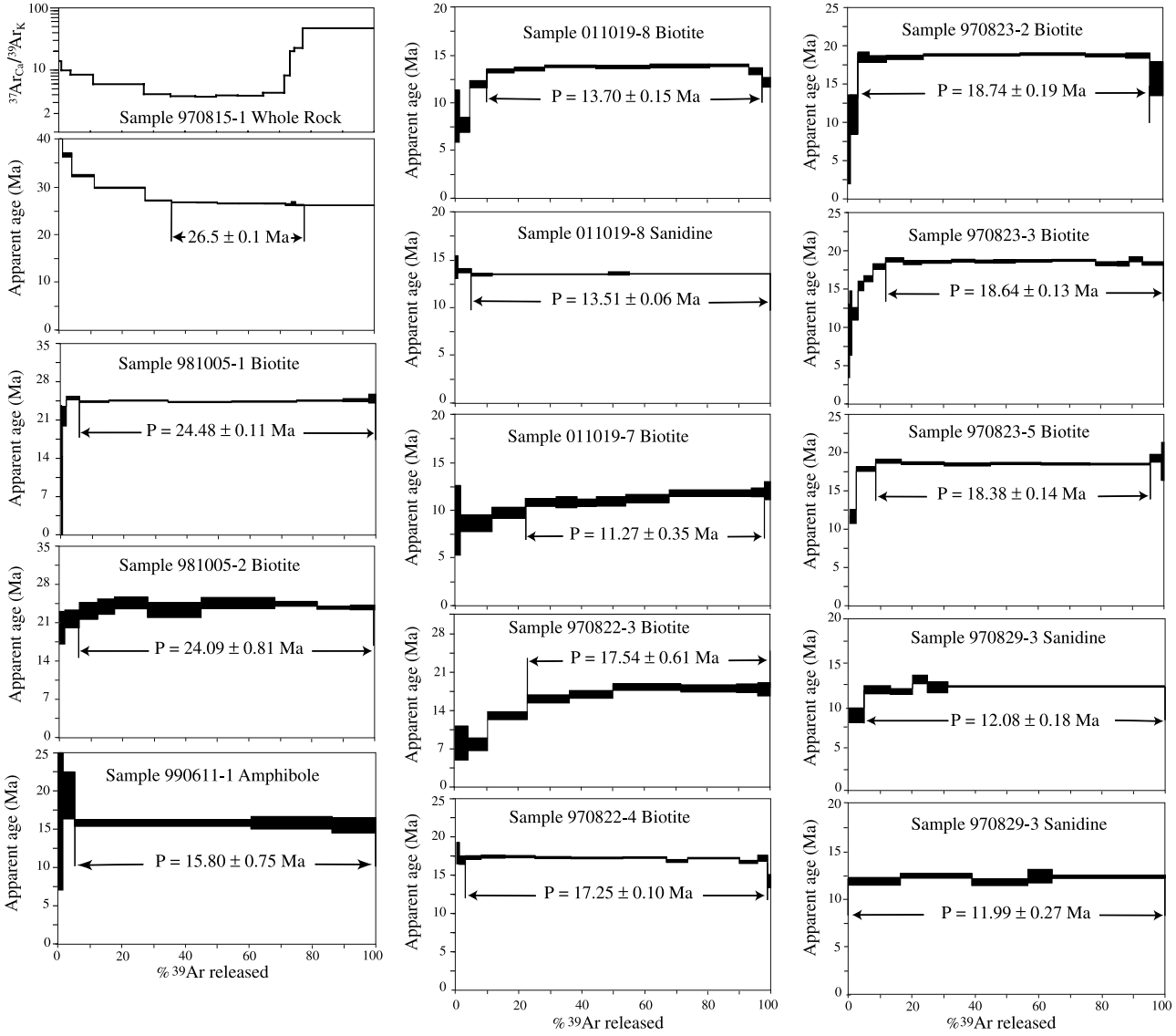

Figure 6. The $^{40}Ar/^{39}Ar$ laser step-heating apparent age spectra. The thickness of the black rectangles corresponds to 1σ uncertainties on the individual ages, while uncertainties on the plateau age are indicated at the 2σ level. For the whole rock sample 970815-1, the Ca/K ratio spectrum, deduced from the isotopic measurement of ^{37}Ar and ^{39}Ar isotopes, reflects compositional variations of the degassed phases and increasing contribution of refractory minerals (e.g., plagioclases and pyroxene) at high temperature.

ing out to define a plateau. This pattern concerns only a small part (<30%) of the total degassed ^{39}Ar and has very little influence on the calculated ages (concordant plateau, isochron and total gas ages, except for 970822-3). This is probably due to a slight alteration of the biotites, whose colors changed from black to glowing bronze during the first few temperature steps.

4. Paleomagnetism

[23] Paleomagnetic samples were collected using a portable gasoline drill and oriented with magnetic and sun compasses, the latter to correct for local declination anomalies. Magnetic remanences were measured with a 2G Inc. three-axis, DC-SQUID magnetometer installed in a magnetically shielded room at the Institut de Physique du Globe de Paris. Samples whose magnetic intensities exceeded 1 A/m were measured with an AGICO JR5 spinner magnetometer. Stepwise (14–22 steps) alternating field (AF) and thermal demagnetization were systematically performed, yet often the presence of high-coercivity minerals rendered AF demagnetization useless. Bulk susceptibility was measured after each heating step for at least half of the samples to monitor potential changes in magnetic mineralogy. Magnetic components were determined using principal component analysis [*Kirschvink*, 1980] except when multiple components with overlapping spectra were present, in which case we used

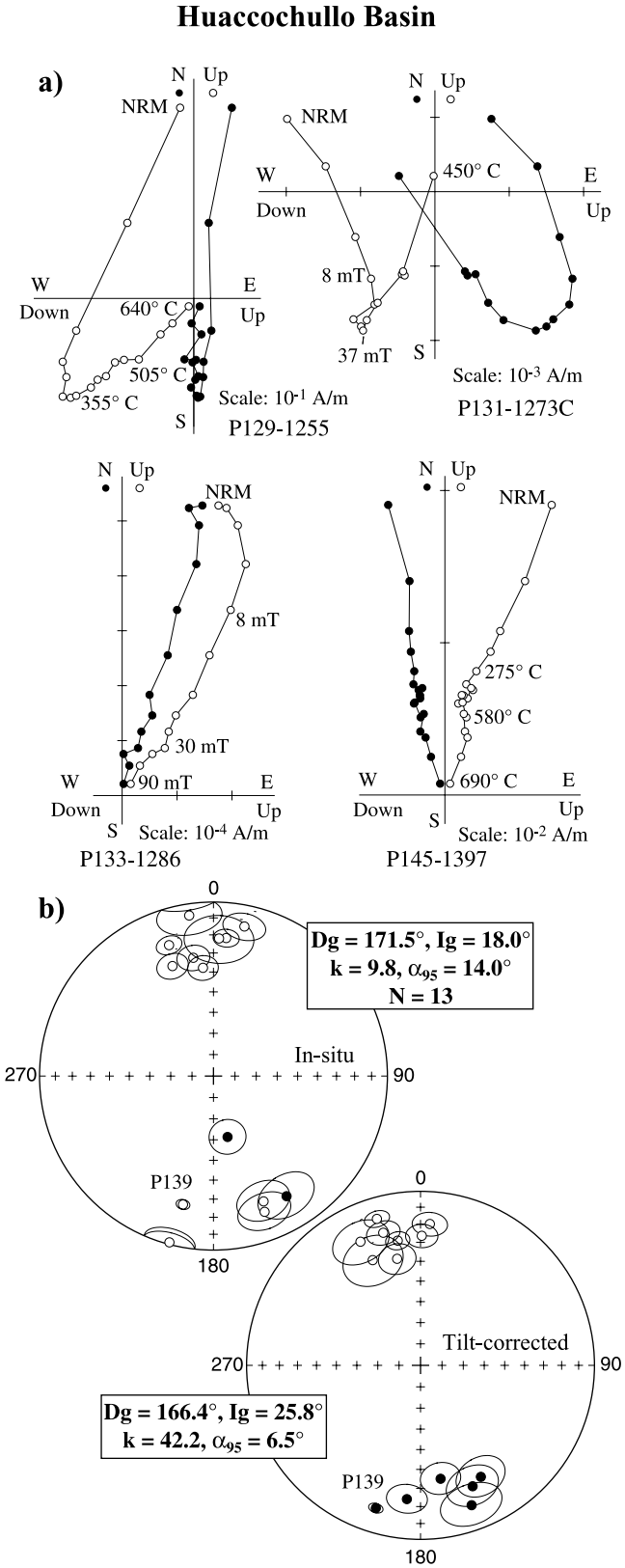

Figure 7. (a) Orthogonal demagnetization diagrams (in situ coordinates) (site and sample numbers, e.g., P129-1255, are below each Zijderveld plot), and (b) equal-area projection of the site mean directions from the Huaccochullo basin.

the remagnetization great circle method [*McFadden and McElhinny*, 1988]. Site-mean directions were calculated using *Fisher* [1953] statistics. The reversal test follows *McFadden and McElhinny* [1990] and the fold test follows *Watson and Enkin* [1993] using 1000 simulations with 5° uncertainties on bedding attitudes. The test statistic is reported at the optimum degree of untilting within 95% confidence level intervals. Data were treated using the software of *Cogné* [2003] and *Enkin* [1995]. Results are listed in Table 3.

4.1. Huaccochullo Basin

[24] For the Pichu Formation, both stepwise thermal and AF demagnetization yielded a stable magnetic component above 400–500°C or 20 mT (Figure 7a), although thermal demagnetization was mostly used due to the common presence of a high-coercivity phase. The Pichu Formation had variable natural remanent magnetization (NRM) intensities ranging from 0.05 to 7 mA/m, occasionally reaching ~100 mA/m (site P129) and more than 1 A/m for the volcanic rocks (site P139). Magnetic mineralogy was highly variable, ranging from titanomagnetite (Curie temperatures lower than 580°C) to ilmeno-hematite (Curie temperatures higher than 580°C but less than 680°C). Demagnetization treatment isolated one or two components (Figure 7a). When present, the low-temperature/coercivity component (LTC) had northerly declinations and shallow inclinations (in situ coordinates), probably reflecting a recent field direction. Both normal and reverse polarities were found for the high-temperature/high-coercivity components (HTC) in roughly equal proportion. For site P139, five samples were collected in sediments, three in an immediately overlying basaltic andesite flow, and two samples in a poorly welded ignimbrite immediately overlying the andesite. The volcanic flows and one sediment sample had a single, very stable component that decayed toward the origin. Three sediment samples possessed overlapping spectra so remagnetization great circles were applied, yielding great circles that coincided with the direction recorded by the volcanic rocks. The very clustered magnetic directions (site mean α_{95} = 2.7°, Table 3) suggest that secular variation was not averaged out and that the sedimentary samples were baked during emplacement of the volcanic rocks. Thus site P139 was omitted from the calculation of the overall mean Pichu Formation direction. The remaining 13 individual site mean directions yield a tilt-corrected overall mean of D_s = 166.4°, I_s = 25.8°, k = 42.2, α_{95} = 6.5° (Table 3). The test statistic maximizes at 85.8 ± 8.7% and the reversal test is positive (class C). Although the fold statistic does not include the 100% unfolding case, the overall mean direction at 85% unfolding (D_s = 170.6°, I_s = 23.1°; k = 26.7, α_{95} = 8.2°) is indistinguishable from the case at 100% unfolding (Table 3). Moreover, the fold test statistic calculated only from the reversed polarity sites (overall mean direction at 100% unfolding: D_s = 164.7°, I_s = 25.9°; k = 33.8, α_{95} = 13.4°, N = 5) maximizes at 99.2 ± 12.3%, indicating that a recent field overprint may not have been completely removed from some normal polarity samples. We thus

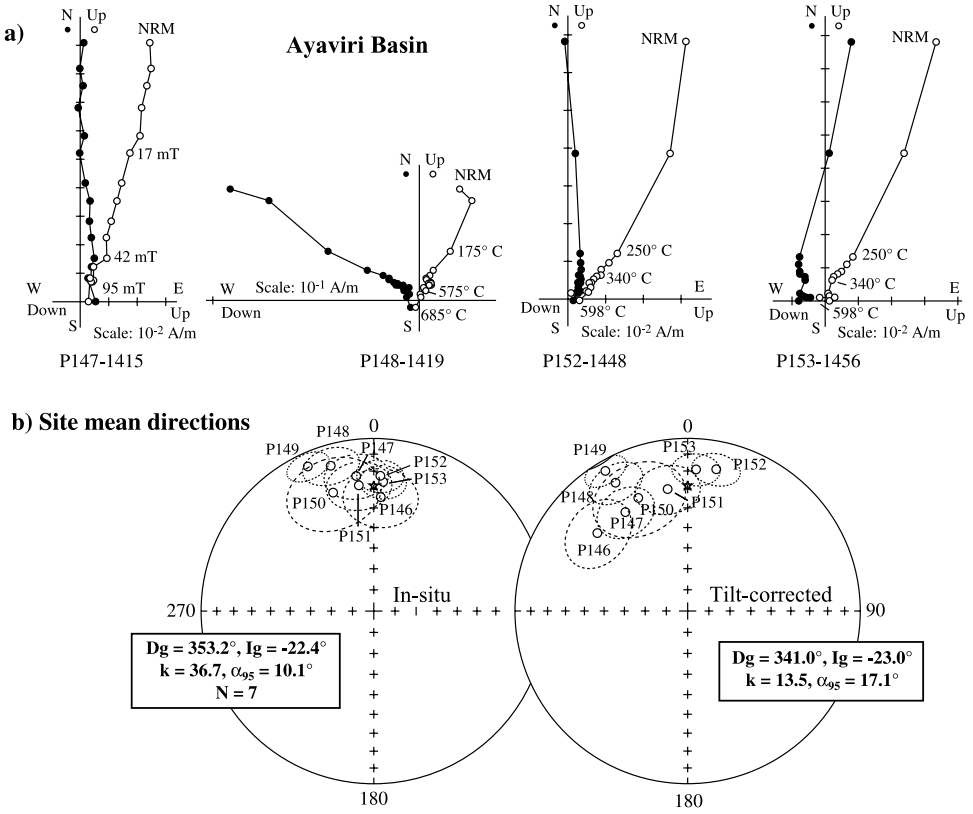

Figure 8. (a) Orthogonal demagnetization diagrams (in situ coordinates) (site and sample numbers, e.g., P147-1415, are below each Zijderveld plot), and (b) equal-area projection of the site mean directions from the Ayaviri basin.

consider the mean direction of 13 sites at 100% unfolding as a primary, prefolding magnetization.

4.2. Ayaviri Basin

[25] The NRM intensities of the Ayaviri basin samples range from 10 to 300 mA/m (excluding site P146, see below). Stepwise thermal and AF demagnetization usually unblocked a single magnetic component above 6 mT or 250°C that persisted until 100 mT or ~580°C, above which the remanent directions became unstable (Figure 8a). The magnetic remanence is principally carried by Fe-rich titanomagnetite, but ~10% of the NRM intensity often persists above 580°C indicating a limited presence of ilmanohematite. The characteristic component decayed toward the origin in only 34% of the samples. All the characteristic component directions (except some from site P146) are of normal polarity and some of the site-mean directions (P146, P152 and P153) lie close to the recent field direction in in situ coordinates (Figure 8b and Table 3). Sample directions from site P150 were very dispersed, with a site mean α_{95} of 19.6°.

[26] Site P146 had directions that decayed univectorally to the origin upon thermal or AF demagnetization. However, the individual sample directions are very scattered, with NRM intensities ranging from 0.034 to 0.078 A/m for the four samples at the bottom of the section (samples 1399–1402) and from 3.8 to 26.2 A/m for the four samples at the top (samples 1403–1406). For the latter, 70% of the magnetization is removed by 20 mT, but not below 540°C. The mean ratio of the NRM moment over the bulk susceptibility is 0.09 for samples 1399–1402 versus 19.2 for 1403–1406. These characteristics, together with their demagnetization behaviors suggest that lightening remagnetized samples 1403–1406. A mean direction was calculated for the three samples with stable magnetizations, however the small number of samples resulted in a site mean α_{95} of 15.7°, which is large but reasonable given the number of samples.

[27] The site mean directions are shown in Figure 8b. The solely normal polarity of all samples (except for one sample in P146) and the negative fold test (−10.6 ± 25.6%) favor the hypothesis of a postfolding and recent age for the magnetization. However, an alternative hypothesis also exists that can explain the data. When observing the site mean directions in tilt corrected coordinates, one notes a systematic progression in declination as a function of stratigraphic position, with the lower beds being more counterclockwise rotated than the upper beds. As the Ayaviri basin is asymmetric, it could be that it rotated counterclockwise during deposition and progressive folding. If true, it would imply that the magnetization was acquired in a normal polarity field within the 16.8–15.5 Ma time window. According to the magneto-

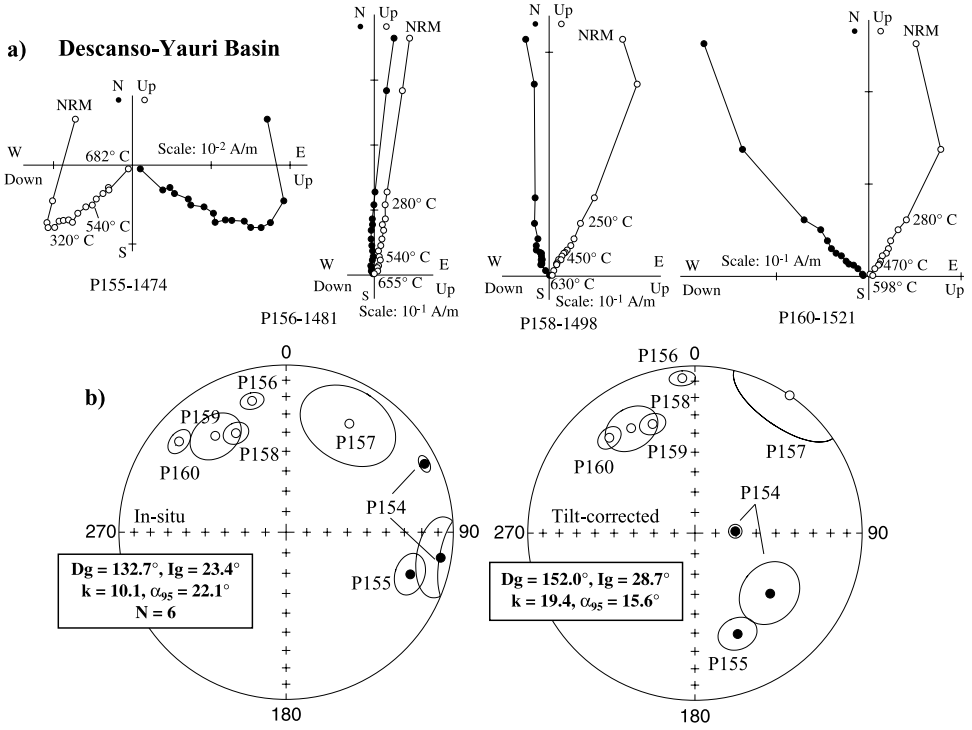

Figure 9. (a) Orthogonal demagnetization diagrams (in situ coordinates) (site and sample numbers, e.g., P155-1474, are below each Zijderveld plot), and (b) equal-area projection of the site mean directions from the Descanso-Yauri basin.

stratigraphic timescale of *Berggren et al.* [1995], the period from 16.8 to 15.5 Ma was dominated by a reverse polarity chron from 15.155 to 16.014 Ma, preceded by five reversals which remained in the normal polarity state much longer (0.610 Ma or 85%) than in the reverse state (0.102 Ma or 15%) until 16.726 Ma. Thus it is not impossible that the sampled horizons were deposited in a normal polarity field between 16.0 and 16.7 Ma, which leads to a reasonable compacted sedimentation rate of ~378 m/Myr. Another argument in favor of this latter hypothesis is that the in situ directions of sites P147, P148, P149 and P151 lie far from the present or axial dipole field directions. Also in agreement with this hypothesis is the systematic rotation of tilt-corrected site mean directions as a function of stratigraphic position (Figure 8b), with the oldest site (P146) recording the greatest amount of counterclockwise rotation (46.9° ± 11.5°) and the youngest site (P153) recording the least (5.7° ± 6.7°). Such a systematic rotation would account for the negative fold test, while conserving the coherency in site mean inclinations (Figure 8b). However, for this latter scenario, one could expect the poles to bedding to be progressively rotated around a vertical axis, which they are not (Figure 5b). Thus two hypotheses can explain the Ayaviri data. One is that the magnetizations are primary, which would imply the Ayaviri basin rotated progressively counterclockwise as the sediments were deposited. The second, more likely hypothesis, is that the magnetizations were overprinted in a normal field.

4.3. Descanso-Yauri Basin

[28] The Descanso-Yauri basin samples have NRM intensities ranging from 0.7 to 680 mA/m with most in the 100–200 mA/m window. They exhibit very stable demagnetization trajectories during stepwise demagnetization that define one or two magnetization components (Figure 9a). An LTC, when present, is removed below 320°C. An HTC is isolated above 320°C that has dual polarities. Site P154 records two significantly distinct populations of directions (Figure 9b). The first one (D_s = 128.8°, I_s = 41.8°, k = 69.8, α_{95} = 14.9°) is carried by three samples, two of reversed polarity situated at the bottom of the 20 m thick section, and one sample of normal polarity at the top of it. The second population consists of five samples lying in the middle of the section (D_s = 87.4°, I_g = 70.3°; k = 538.5, α_{95} = 3.3°) that possess magnetization intensities an order of magnitude lower than the first. One possible interpretation of these directions, in agreement with the stratigraphic position of the samples, is that this site recorded a magnetic field reversal, with the three samples above and below representing the dipole field while the five others recorded a transitional field. Site P157 had very well defined but highly dispersed individual directions resulting in an α_{95} close to 20°. The origin of this scatter remains unknown

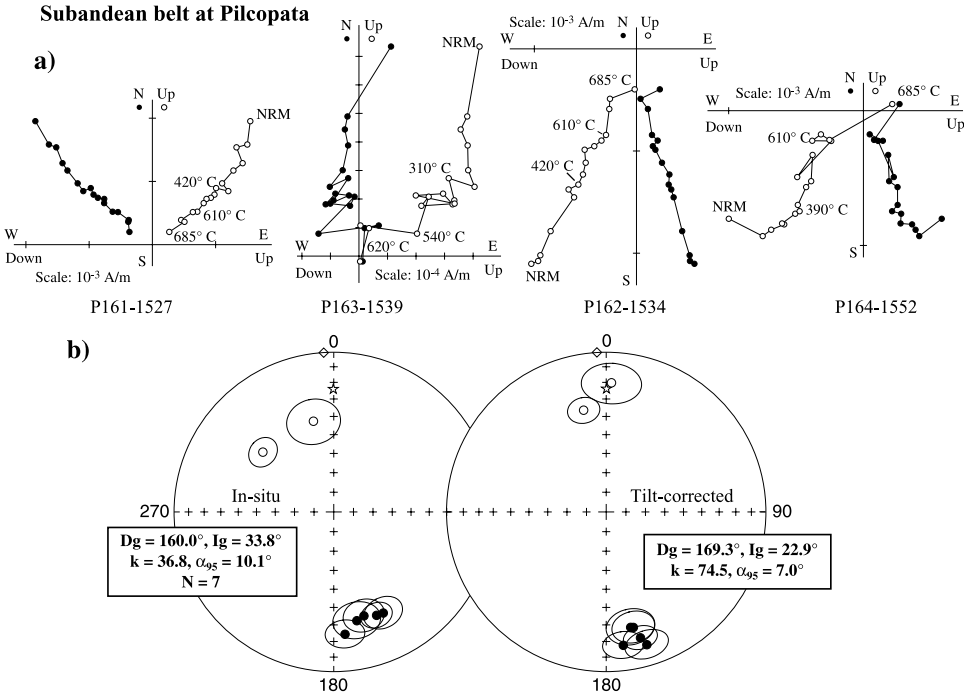

Figure 10. (a) Orthogonal demagnetization diagrams (in situ coordinates) (site and sample numbers, e.g., P161-1527, are below each Zijderveld plot), and (b) equal-area projection of the site mean directions from the Ipururo Formation (Pilcopata, sub-Andean belt).

and this site was omitted from further consideration. Applying the fold test on the six site mean directions yields a test statistic maximum at 123.6 ± 24.7% unfolding yet the uncertainty about the mean is high (D_s = 152.0°, I_s = 28.7°, k = 19.4, α_{95} = 15.6°). Although P156 has a well-defined site mean direction, it is different at the 95% confidence level from the other five remaining sites. Considering it as an outlier and using the remaining five site mean directions to calculate an overall mean direction gives D_s = 146.6°, I_s = 32.3°, k = 42.0, α_{95} = 11.9°. The fold test statistic maximizes at 114.1 ± 20.6%. Two samples from site P154 and nine from site P155 have reversed polarity, clearly antipodal to the others; a positive reversal test is obtained at the sample level (class B). The overall mean directions based on N = 5 and 6 sites are similar, yet we prefer the one based on 5 sites due to its lower uncertainty.

4.4. Sub-Andean Belt at Pilcopata

[29] The Ipururo Formation red sandstones present relatively low and homogeneous NRM intensities (0.3–3.3 mA/m) (Figure 10). From the pilot study results, we used mainly thermal demagnetization, as AF demagnetization often resulted in incomplete demagnetization due to the presence of high-coercivity minerals. The magnetic remanence is principally carried by titanomagnetite, but for some sites (P161, P162 and P164) ~25–40% of the NRM intensity persists above 580°C indicating the presence of ilmeno-hematite. Stepwise thermal demagnetization mostly isolated two magnetic components, a low-temperature/coercivity component probably of viscous origin and a high-temperature/coercivity component (HTC) that appears generally above 250°–330°C. Fairly noisy HTC directions were found mostly in sites where the remanence was carried by titanomagnetite (P165–P167) as reflected in their corresponding site mean α_{95}s on the order of 10° (Table 3). The overall tilt-corrected site mean direction based on seven sites passes the reversal test (class C), and the fold test statistic maximizes at 83 ± 35% (Table 3). Despite the large confidence interval, the fold test statistic includes the case at 100% unfolding, and combined with the positive reversal test and the fact that the in situ site mean directions do not include the expected Bruhnes or recent field directions, favors the interpretation of a prefolding, primary magnetization for these rocks.

5. Interpretation and Discussion

5.1. Synthesis of Paleomagnetic and Geochronologic Results

[30] In order to draw tectonic inferences, paleomagnetic vertical axis rotations were calculated by comparing the overall mean pole for each locality with the reference pole of the equivalent age from the synthetic South American apparent polar wander path (APWP) of *Besse and Courtillot* [2002]. For the Altiplano basins, $^{40}Ar/^{39}Ar$ dating precisely defined the age of the sampled strata, and hence allows us to compare against the reference pole of the appropriate age. The Ipururo Formation from the sub-Andean belt is broadly constrained as Miocene, yet older than 9 Ma.

[31] The $^{40}Ar/^{39}Ar$ dating in the Huaccochullo basin defines two distinct populations, with older ages in the northwestern part of the basin (26.5–24.0 Ma, sites P143–P145, Table 3) and younger ones in the southeast (13–12 Ma, sites P129–P134 and P138–P142, Table 3). The overall tilt-corrected mean paleomagnetic directions of the two are identical at the 95% significance level (D_s = 169.2°, I_s = 20.7°, α_{95} = 17.2°, N = 3 versus Ds = 165.5°, Is = 27.3°, α_{95} = 7.8°, N = 10). We thus combined the two populations for further interpretation. Comparing the overall mean pole (76.6°S, 28.9°E, A_{95} = 6.1°) against the 20 Ma reference pole (84.7°S, 313.8°E, A_{95} = 2.7°) suggests that the Huaccochullo basin experienced a significant counterclockwise rotation of 11.3° ± 5.4°.

[32] The paleomagnetic results for the Ayaviri basin may represent a recent remagnetization because, except for one sample, solely normal polarities are found and because the site mean directions are better grouped in the in situ reference frame. Alternatively, the magnetizations could have been acquired in a very short time period (<1 Myr), during infilling of the asymmetric basin as it progressively deformed and rotated about a vertical axis. Presently, the most conservative explanation for the Ayaviri basin sediments is that they are overprinted. More work is needed to fully understand the paleomagnetic data from this basin.

[33] For the Descanso basin, the $^{40}Ar/^{39}Ar$ data bracket the age of the sampled strata between 18.5 and 12.1 Ma. Six sites from this basin pass the fold and reversal tests and likely possess primary remanent magnetizations. Despite this, one site lies far from the rest and adds a few degrees of uncertainty to the result. We thus omitted this site when calculating an overall mean pole for the Descanso basin (57.6°S, 8.4°E, A_{95} = 12.2°, N = 5), which yields a 31.0° ± 10.2° counterclockwise rotation versus the 20 Ma reference pole for stable South America (84.7°S, 313.8°E, A_{95} = 2.7°).

[34] In the sub-Andean belt, the overall mean pole based on seven sites (79.5°S, 21.0°E, A_{95} = 5.7°) compared to the 10 Ma reference pole (85.9°S, 331°E, A_{95} = 2.0°) implies a counterclockwise rotation of 7.8° ± 4.8°. The rotation magnitude does not change significantly when compared against the 20 Ma pole (8.3° ± 5.1° counterclockwise). This amount of rotation is similar to, yet slightly less than, that of the Huaccochullo basin some 300 km to the south, on the other side of the Eastern Cordillera.

5.2. Tectonics of the Northern Bolivian Orocline

[35] The Neogene paleomagnetic data described herein help constrain the deformation history of the northern Bolivian Orocline, a vast region previously void of such data (Figure 2). The large area covered by the 13 sites (~5000 km^2) from the Huaccochullo basin leads to the interpretation that this rotation is regional in scope and younger than 12 Ma in age, with little or no differential rotation occurring from circa 26 to 12 Ma. Moreover, the Huaccochullo basin result is remarkably consistent with a ~10° counterclockwise rotation found in 14–9 Ma sediments from the Corque basin in the central Altiplano (Figure 4) [*Roperch et al.*, 1999], both being situated above the symmetry axis of the Bolivian Orocline as defined by *Gephart* [1994]. It is possible that they rotated as a rigid block, yet the internal deformation experienced by both basins makes this hypothesis unlikely.

[36] Less clear is whether the rotation in the sub-Andean belt at Pilcopata occurred simultaneously with, or postdates, the rotation of the Huaccochullo basin. The latter suggests a west to east propagation of deformation, with the rotation in the Huaccochullo basin preceding that in the sub-Andean belt. The former could imply that the northern Bolivian Orocline experienced a wholesale ~10° counterclockwise rotation in the last ~12 Myr with (1) the adjacent sub-Andean belt rotating with the northern Bolivian Orocline, meaning that the rotation must be accommodated along a fault east of the sub-Andean belt, or (2) the rotation at Pilcopata is due to local, thin-skinned tectonics, decoupled from the thick-skinned deformation farther west. To our knowledge, there is no evidence to suggest the existence of a major structure to facilitate the wholesale rotation of the northern Bolivian Orocline and the adjacent sub-Andean belt, thus option 1 is easily dismissed. Although the relatively limited area of the Pilcopata locality may not be representative of the entire sub-Andean belt from 12° to 17°S, *Lamb* [2001] and *Richards et al.* [2004] actually predicted 5°–10° counterclockwise rotations in the last 10 Myr in that area (Figures 3c and 3d), whereas *Kley* [1999] predicted no rotation (Figure 3b). More paleomagnetic data are needed to resolve this question.

[37] The 31° counterclockwise rotation of the Descanso-Yauri basin likely occurred around 12 Ma, during or just after deformation of the sediments. If the entire northern Altiplano experienced a 10° counterclockwise rotation, then the Descanso basin must have absorbed an additional shear component to account for its larger rotation, e.g., a 10° counterclockwise rotation of the northern Altiplano plus a 20° counterclockwise rotation due to an additional shear component. This is compatible with deformation features measured along bounding faults that indicate sinistral strike-slip acted within an overall E-W directed stress regime [*Cerpa and Meza*, 2001]. The local stress field and fault pattern acting in this basin might have led to an isolated region accommodating greater shear and concomitant rotation. However, the Descanso basin lies in a southeast trending zone spanning from Cusco to Puno and beyond that contains older rocks also possessing large counterclockwise rotations (Figures 2, 4, and 5b). For example, 10 sites of Eocene rocks were found to be rotated ~15°–80° counterclockwise [*Butler et al.*, 1995] (Figure 2) and 19 sites of Late Permian to Early Jurassic rocks were found to be rotated 14°–147° counterclockwise [*Roperch and Carlier*, 1992; *Gilder et al.*, 2003]. This zone, mapped as the SFUACC left-lateral shear zone, is identified as an important tectonic feature of the northern limb of the Bolivian Orocline [*Sempere et al.*, 2002b; *Carlier et al.*, 2005]. Moreover, growth strata in the Descanso and Ayaviri basins are coeval (18.5–12.1 Ma versus 16.8–15.5 Ma), suggesting both basins were influenced by the same tectonic regime. Thus it seems that the

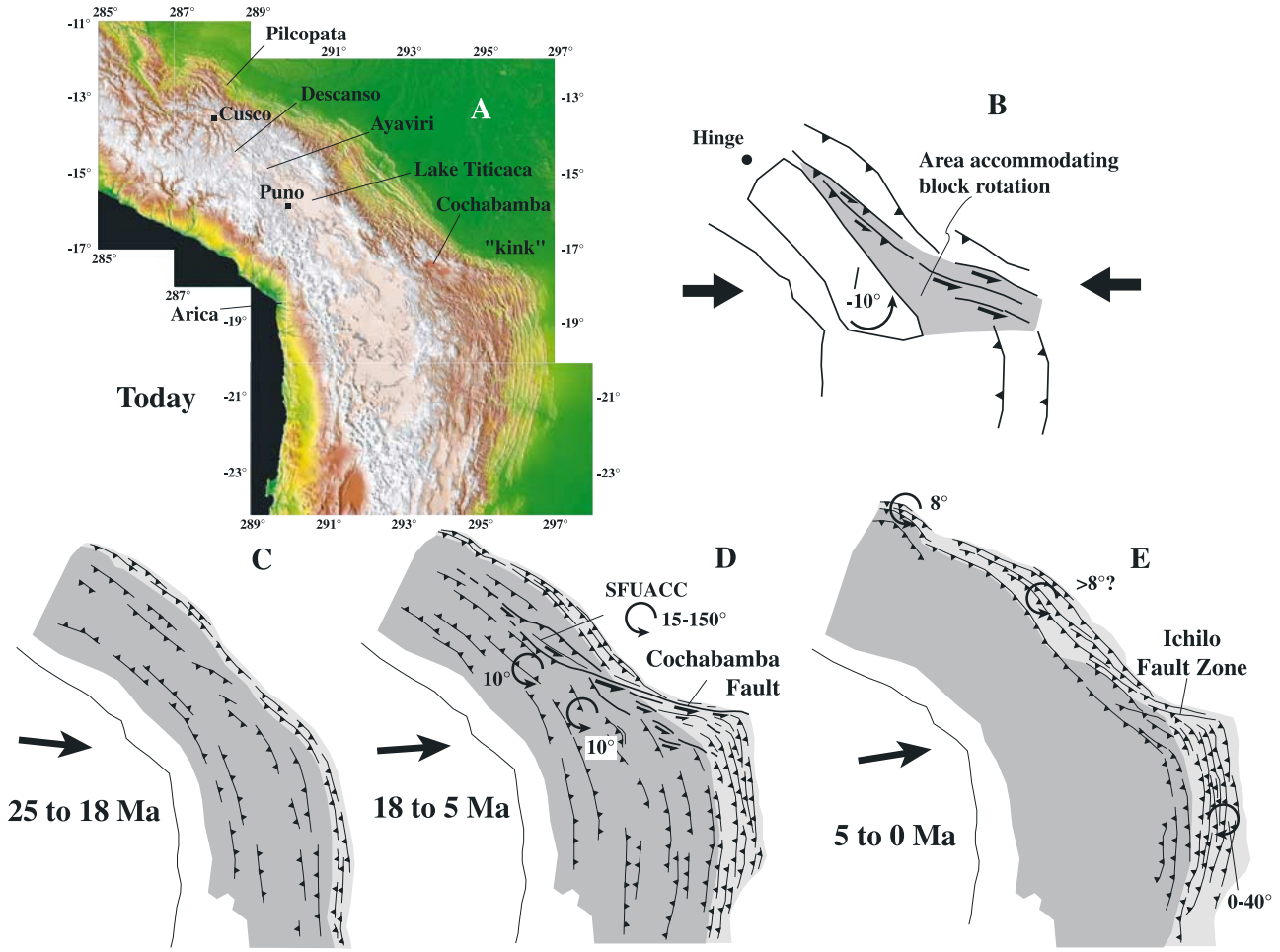

Figure 11. Tectonic model of the northern Bolivian Orocline and the origin of the kink in the sub-Andean belt. (a) SRTM digital elevation model. (b) General model proposed to explain the tectonic evolution of the northern Bolivian Orocline. A large region that rotated 10° counterclockwise, more or less coherently, about a pole of rotation located to the northwest is shown. To the southeast, the rotation is accommodated mostly by left-lateral strike-slip motion on WNW trending faults. Farther north, where the structures trend NW, the rotation is accommodated primarily by shortening with a minor component of left-lateral shear. (c) From 25 to 18 Ma, a time of intense deformation both within, yet mostly at the margins of, the Altiplano. A thin proto-sub-Andean belt is inferred to the east. (d) From 18 to 5 Ma, corresponding to the time of major motion on the SFUACC-Cochabamba left-lateral shear zone (thick lines) and a regional 10° counterclockwise rotation of the northern Altiplano (see Figure 11b for general explanation). Left-lateral motion on the SFUACC-Cochabamba fault system accounts for a much thicker sub-Andean belt to the south of the fault (18°S) than to the north, giving rise to the kink and to the widespread counterclockwise rotations observed within the SFUACC (see text). (e) From 5 Ma to Present, deformation ceases within the Altiplano and mostly within the Eastern Cordillera. Much of the compressive deformation shifts to the sub-Andean belt both north and south of 18°S. Counterclockwise rotation north of 18°S, and clockwise or no rotation south of 18°S, follows the suggestions of previous models (Figure 3). In Figures 11c–11e, light gray shading corresponds to the sub-Andean belt, while dark gray shading represents topography in excess of 3000 m.

31° counterclockwise rotation in the Descanso basin is compatible with the interpretation that this basin (and the Ayaviri basin) formed within a left-lateral shear zone (the SFUACC).

[38] That all three regions possess significant counterclockwise rotations has been anticipated by most kinematic models of deformation for the northern Bolivian Orocline (Figure 3). Our new results imply that the curvature of the northern Altiplano was enhanced by ~10° in the last 12 Myr, which is generally consistent with the kinematic models of *Isacks* [1988] and *Kley* [1999]. If true, all pre-12 Ma rocks between the Western and Eastern cordillera should record minimum counterclockwise rotations of 10°, which is consistent with the limited available data

(Figure 2). On the other hand, paleomagnetic rotations do not correlate with fold axis trends (Figures 2, 4, and 5 and Table 3), which argues against a simplistic oroclinal bending model [*Carey*, 1955]. The bulk of our data are coherent with a broad region including the Huaccochullo and Corque basins that deformed and rotated more or less coherently, while the region directly east (e.g., the SFUACC) accommodated the bulk of the shear component associated with the large block rotation.

[39] The sum of these observations leads us to advocate a model, shown in Figure 11, for the tectonic evolution of the northern Bolivian Orocline since 25 Ma. Figure 11b presents the main idea, which is a region undergoing a 10° counterclockwise rotation about a pole of rotation located outside the block to its northwest. This requires more space to accommodate the block rotation to the south than to the north, which is accomplished by an increasing gradient in the amount of lateral movement, via left-lateral strike slip, toward the south as the faults change trend from NW to WNW. NW trending faults toward the north take up the rotation mostly by shortening. In this way, the model falls close to that in Figure 3b, except that the block rotates according to an Euler pole to the northwest, as proposed in Figure 3d.

[40] A sequence of cartoons, shown in Figures 11c–11e, more precisely defines the model in space and time. Again, we are concerned mostly with the northern Bolivian Orocline; more details for the region south of 19°S are given by, for example, *Hérail et al.* [1996], *Allmendinger et al.* [1997], *Jordan et al.* [1997], *Lamb et al.* [1997], *Lamb* [2001], *Müller et al.* [2002] and *Riller and Oncken* [2003, and references therein]. Between 25 and 18 Ma (Figure 11c), deformation occurred both within, yet mostly at the margins of, the Altiplano [e.g., *Kennan et al.*, 1995; *Lamb et al.*, 1997; *Kennan*, 2000; *Müller et al.*, 2002]. In the Bolivian sub-Andes, clastic sequences were deposited from ~27 to 10 Ma, ending a 40 Myr hiatus [*Sempere et al.*, 1990; *Marshall et al.*, 1993]. Therefore we postulate the presence of a thin, continuous sub-Andean belt from 25 to 18 Ma.

[41] The period from 18 to 5 Ma represents the onset of intense deformation through the entire Altiplano (Figure 11d) [*Allmendinger et al.*, 1997; *Lamb et al.*, 1997; *Kennan*, 2000; *Victor et al.*, 2004, and reference therein]. According to *Lamb and Hoke* [1997], the WNW trending Eucalyptus fault zone in Bolivia (Figure 4) was active in the early to middle Miocene and formed the main eastern boundary of the Altiplano basin. This is coincident with the timing of transpressional movement along the SFUACC. Here we link the SFUACC with the Cochabamba fault to form a large left-lateral strike-slip system because they were active simultaneously (at least partly), they have the same sense of offset, and together they can explain the characteristic kink at the eastern border of the Andes around 18°S as well as the widespread rotation of the Altiplano. The existence of the SFUACC was postulated in early regional studies as a continuation of the Tunari (now called Cochabamba) fault system that extends from the major kink in the Bolivian sub-Andean belt [*Newell*, 1949; *Rod*, 1960] (Figures 4 and 11). Offset markers, the existence of small pull-apart basins and earthquake focal mechanisms all indicate that the Cochabamba fault system accommodated(s) left lateral strike-slip motion [*Dewey and Lamb*, 1992; *Sheffels*, 1995; *Kennan et al.*, 1995; *Kley*, 1999; *Müller et al.*, 2002]. Specifically, satellite image analyses led *Allenby* [1987] to propose that a maximum of 80 kilometers of left-lateral motion took place along the E-W trending Ichilo (Cochabamba) fault zone. Paleomagnetic studies in the Cochabamba area have thus far revealed a complex pattern of rotations in Cretaceous and Paleocene rocks (Figure 2) [*Lamb*, 2001; *Richards et al.*, 2004]; local paleomagnetic rotations with a range in magnitudes are common to strike-slip environments [e.g., *Luyendyk et al.*, 1985]. On the basis of the convergence direction acting at the time (Figure 11d), the SFUACC-Cochabamba fault system would have primarily accommodated shortening to the north, where the fault trends NW, and left-lateral strike-slip motion to the south, where the faults trend WNW. Motion on the SFUACC-Cochabamba fault can also help accommodate the 10° counterclockwise rotation of the northern Altiplano. As this lithospheric-scale fault propagated east, thrusting in the ramp anticlines in the sub-Andean belt would absorb left-lateral strike slip motion. Left-lateral offset on the SFUACC-Cochabamba fault system would be a maximum (80 km) near the center of the fault then diminish to the east and north (as represented by reduced arrow size in Figure 11d). Such a scenario accounts for the difference in age and tectonic style of the sub-Andean belt north and south of the kink [*Horton*, 1999], with the southern part being much thicker, older, and better developed than the north. For example, *Baby et al.* [1997] and *Lamb and Hoke* [1997] suggested shortening amounts total ~190 km in the north and closer to 240 in the south. Using balanced cross sections, *McQuarrie* [2002] found a ~30 km difference in shortening between the two regions, with more shortening to the south.

[42] Deformation in the Altiplano and Eastern Cordillera ceased around 5 Ma (Figure 11e), consistent with the observations that ignimbrites and ancient peneplain surfaces there are largely undeformed [*Gubbels et al.*, 1993; *Kennan et al.*, 1995]. Deformed sequences as young as 9 Ma are overlain with a marked angular unconformity by flat lying 3–5 Ma ignimbrites [*Marshall et al.*, 1993]. Our model suggests that deformation in the last 5 Myr has been restricted mostly to the sub-Andean fold and thrust belt, with shortening amounts both north and south of 17°S being relatively homogeneous. We postulate that it is during this latest stage that the section around Pilcopata was rotated.

[43] Despite the clear limitations of the tectonic model, our combined paleomagnetic and radiochronologic data strongly support the existence of widespread deformation acting across the northern Altiplano in the middle to late Miocene. These data emphasize the importance of sinistral transpression in accommodating the deformation. We think that an important consequence of large-scale sinistral faulting is the creation of the kink in the sub-Andean belt. Continued sampling and data acquisition are necessary and

will surely refine the tectonic history of the Bolivian Orocline region proposed herein.

[44] **Acknowledgments.** We thank Dan Farber for introducing S.G. and S.R. to Peruvian geology, Victor Torres and Wilber Hermoza for their help in the field, and the IRD delegation in Lima for their logistical support. This research was supported by INSU-CNRS program Interieur de la Terre. Constructive reviews by Ulrich Riller and Pierrick Roperch significantly improved the quality of this manuscript. We also thank Onno Oncken for his patience. Contribution UMR Geosciences Azur 751 and IPGP 2060.

References

Abels, A., and L. Bischoff (1999), Clockwise block rotations in northern Chile: Indications for a large-scale domino mechanism during the middle-late Eocene, *Geology*, *27*, 751–754.

Allenby, R. J. (1987), Origin of the Bolivian Andean Orocline: A geologic study utilizing Landsat and Shuttle imaging radar, *Tectonophysics*, *142*, 137–154.

Allmendinger, R. W., T. E. Jordan, S. M. Kay, and B. L. Isacks (1997), The evolution of the Altiplano-Puna plateau of the central Andes, *Annu. Rev. Earth Planet. Sci.*, *25*, 139–174.

Aubry, L., P. Roperch, M. de Urreiztieta, E. Rossello, and A. Chauvin (1996), Paleomagnetic study along the southeastern edge of the Altiplano-Puna Plateau: Neogene tectonic rotations, *J. Geophys. Res.*, *101*, 17,883–17,900.

Audebaud, E., et al. (1973), Les traits Géologiques essentiels des Andes centrales (Pérou-Bolivie), *Rev. Géogr. Phys. Geol. Dyn.*, *15*, 73–113.

Babeyko, A. Y., S. V. Sobolev, R. B. Trumbull, O. Oncken, and L. L. Lavier (2002), Numerical models of crustal scale convection and partial melting beneath the Altiplano-Puna plateau, *Earth Planet. Sci. Lett.*, *199*, 373–388.

Baby, P., P. Rochat, G. Mascle, and G. Hérail (1997), Neogene shortening contribution to crustal thickening in the back arc of the central Andes, *Geology*, *25*, 883–886.

Beck, M. E. (1988), Analysis of Late Jurassic-Recent paleomagnetic data from active plate margins of South America, *J. S. Am. Earth Sci.*, *1*, 39–52.

Beck, M. E. (1998), On the mechanism of crustal block rotations in the central Andes, *Tectonophysics*, *299*, 75–92.

Beck, S. L., G. Zandt, S. C. Myers, T. C. Wallace, P. G. Silver, and L. Drake (1996), Crustal-thickness variations in the central Andes, *Geology*, *24*, 407–410.

Berggren, W. A., D. V. Kent, C. C. Swisher, and M. P. Aubry (1995), A revised Cenozoic geochronology and chronostratigraphy in time scales and global stratigraphic correlations: A unified temporal framework for an historical geology, in *Geochronology, Time-scales, and Stratigraphic Correlation*, edited by W. A. Berggren, D. V. Kent, M.-P. Aubry, and J. Hardenbol, *Spec. Publ. SEPM Soc. Sediment. Geol.*, *54*, 129–212.

Besse, J., and V. Courtillot (2002), Apparent and true polar wander and the geometry of the geomagnetic field over the last 200 Myr, *J. Geophys. Res.*, *107*(B11), 2300, doi:10.1029/2000JB000050.

Boudesseul, N., M. Fornari, T. Sempere, G. Carlier, M. Mamani, I. Ibarra, P. Meza, and L. Cerpa (2000), Un importante evento volcánico de edad Mioceno inferior en la zona de Descanso–Ayaviri–Condoroma–Santa Lucía (Dptos. de Cusco, Puno y Arequipa), in *X Congreso Peruano de Geología*, p. 8 and CD-ROM file GR6A (9 pp.), Geol. del Perú, Lima.

Brasse, H., P. Lezaeta, V. Rath, K. Schwalenberg, W. Soyer, and V. Haak (2002), The Bolivian Altiplano conductivity anomaly, *J. Geophys. Res.*, *107*(B5), 2096, doi:10.1029/2001JB000391.

Butler, R. F., D. R. Richards, T. Sempere, and L. G. Marshall (1995), Paleomagnetic determinations of vertical-axis tectonic rotations from late Cretaceous and Paleocene strata of Bolivia, *Geology*, *23*, 799–802.

Campbell, K. E., Jr., M. Heizler, C. D. Frailey, L. Romero-Pittman, and D. R. Prothero (2001), Upper Cenozoic chronostratigraphy of the southwestern Amazon Basin, *Geology*, *29*, 595–598.

Carey, S. W. (1955), The orocline concept in geotectonics, *Proc. R. Soc. Tasmania*, *89*, 255–288.

Carlier, G., J. P. Lorand, J. P. Liégeois, M. Fornari, P. Soler, V. Carlotto, and J. Cárdenas (2005), Potassic-ultrapotassic mafic rocks delineate two lithospheric mantle blocks beneath the southern Altiplano, *Geology*, *33*, 601–604.

Cerpa, L., and P. Meza (2001), Las cuencas neogenas del sur del Perú: La cuenca Descanso-Yauri (Mioceno). Evolución sedimentológica y tectónica, Tesis de grado thesis, 114 pp., Univ. Nac. San Antonio Abad del Cusco, Cuzco, Bolivia.

Cerpa, L., P. Meza, V. Carlotto, M. Fornari, and T. Sempere (2004), Paleogeografía y evolución de la cuenca miocena de Descanso-Yauri (Cusco), in *Nuevas contribuciones del IRD y sus contrapartes al conocimiento geológico del sur del Perú*, *Publ. Espec.5*, edited by J. Jacay and T. Sempere, pp. 175–182, Soc. Geol. del Perú, Lima.

Cogné, J. P. (2003), PaleoMac: A Macintosh™ application for treating paleomagnetic data and making plate reconstructions, *Geochem. Geophys. Geosyst.*, *4*(1), 1007, doi:10.1029/2001GC000227.

Coutand, I., P. R. Cobbold, M. d. Urreiztieta, P. Gautier, A. Chauvin, D. Gapais, E. A. Rossello, and O. Lopez-Gamundi (2001), Style and tectonic history of Andean deformation, Puna plateau, northwestern Argentina, *Tectonics*, *20*, 210–234.

Cuéllar, E. (2001), Estratigrafía, sedimentología y tectónica de las series meso-cenozoicas de cuadrángulo de Pichacani (hoja 33–y, cuadrante SE), sur del Perú, Tesis de grado thesis, 86 pp., Univ. Nacional de San Antonio Abad del Cusco, Cuzco, Bolivia.

DeCelles, P. G., and B. K. Horton (2003), Early to middle Tertiary foreland basin development and the history of Andean crustal shortening in Bolivia, *Geol. Soc. Am. Bull.*, *115*, 58–77.

Demets, C., R. G. Gordon, D. F. Argus, and S. Stein (1994), Effect of recent revisions to the geomagnetic reversal time scale on estimates of current plate motions, *Geophys. Res. Lett.*, *21*, 2191–2194.

Dewey, J. F., and S. H. Lamb (1992), Active tectonics of the Andes, *Tectonophysics*, *205*, 79–95.

Dorbath, L., C. Dorbath, E. Jimenez, and L. Riviera (1991), Seismicity and tectonic deformation in the Eastern Cordillera and the sub-Andean zone of central Peru, *J. S. Am. Earth Sci.*, *4*, 13–24.

Enkin, R. J. (1995), A computer program package for analysis and presentation of paleomagnetic data-PMSTAT, vol. 1995, Pac. Geosci. Cent., Geol. Surv. of Can., Sidney, B. C.

Fisher, R. A. (1953), Dispersion on a sphere, *Proc. R. Soc. London*, *217*, 295–305.

Fornari, M., M. Mamani, I. Ibarra, and G. Carlier (2002), Datación del período volcánico "Tacaza" en el Altiplano de Perú y Bolivia, paper presented at XI Congreso Peruano de Geología, Geol. del Perú, Lima.

Gephart, J. W. (1994), Topography and subduction geometry in the central Andes: Clues to the mechanics of a noncollisonal orogen, *J. Geophys. Res.*, *99*, 12,279–12,288.

Gilder, S., S. Rousse, D. Farber, B. McNulty, T. Sempere, V. Torres, and O. Palacios (2003), Post-Middle Oligocene origin of paleomagnetic rotations in the Upper Permian to Lower Jurassic rocks from northern and southern Peru, *Earth Planet. Sci. Lett.*, *210*, 233–248.

Gubbels, T. L., B. L. Isacks, and E. Farrar (1993), High-level surfaces, plateau uplift, and foreland development, Bolivian central Andes, *Geology*, *21*, 695–698.

Hérail, G., J. Oller, P. Baby, M. G. Bonhomme, and P. Soler (1996), Strike-slip faulting, thrusting and related basins in the Cenozoic evolution of the southern branch of the Bolivian Orocline, *Tectonophysics*, *259*, 201–202.

Hindle, D., J. Kley, O. Oncken, and S. Sobolev (2005), Crustal balance and crustal flux from shortening estimates in the central Andes, *Earth Planet. Sci. Lett.*, *230*, 113–124.

Horton, B. K. (1999), Erosional control on the geometry and kinematics of thrust belt development in the central Andes, *Tectonics*, *18*, 1292–1304.

Horton, B. K., B. A. Hampton, and G. L. Waanders (2001), Paleogene synorogenic sedimentation in the Altiplano plateau and implications for initial mountain building in the central Andes, *Geol. Soc. Am. Bull.*, *113*, 1387–1400.

Husson, L., and T. Sempere (2003), Thickening the Altiplano crust by gravity-driven crustal channel flow, *Geophys. Res. Lett.*, *30*(5), 1243, doi:10.1029/2002GL016877.

Isacks, B. L. (1988), Uplift of the central Andean Plateau and bending of the Bolivian Orocline, *J. Geophys. Res.*, *93*, 3211–3231.

Ibarra, I., M. Mamani, R. Rodríguez, T. Sempere, V. Carlotto and G. Carlier (2004), Estratigrafía y tectónica de la parte sur de la cuenca de Ayaviri, in *Nuevas contribuciones del IRD y sus contrapartes al conocimiento geológico del sur del Perú*, *Publ. Espec. 5*, edited by J. Jacay and T. Sempere, pp. 143–155, Soc. Geol. del Perú, Lima.

Jacay, J., and T. Sempere (Eds.) (2004), *Nuevas contribuciones del IRD y sus contrapartes al conocimiento geológico del sur del Perú*, *Spec. Publ. 5*, Soc. Geol. del Perú, Lima.

Jacay, J., T. Sempere, L. Husson, and A. Pino (2002), Structural characteristics of the Incapuquio fault system, southern Peru, paper presented at 5th International Symposium of Andean Geodynamics, Inst. de Rech. pour le Dév., Lima.

James, D. E. (1971), Andean crustal and upper mantle structure, *J. Geophys. Res.*, *76*, 3246–3271.

James, D. E., and I. S. Sacks (1999), Cenozoic formation of the central Andes: A geophysical perspective, in *Geology and Ore Deposits of the central Andes*, *Spec. Publ. 7*, edited by B. J. Skinner, pp. 1–25, Soc. of Econ. Geol., Richardson, Tex.

Jordan, T., J. H. Reynolds, and J. P. Erikson (1997), Variability in age of initial shortening and uplift in the central Andes, 16–33°30′S, in *Tectonic Uplift and Climate Change*, edited by W. F. Ruddiman, pp. 41–61, Springer, New York.

Jordan, T., M. W. Burns, R. Veiga, F. Pangaro, P. Copeland, S. Kelley, and C. Mpodozis (2001), Extension and basin formation in the southern Andes caused by increased convergence rate: A mid-Cenozoic trigger for the Andes, *Tectonics*, *20*, 308–324.

Jordan, T. E., B. L. Isacks, R. W. Allmendinger, J. A. Brewer, V. A. Ramos, and C. J. Ando (1983), Andean Tectonics related to geometry of the subducted Nazca plate, *Geol. Soc. Am. Bull.*, *94*, 341–361.

Kaneoka, I., and C. Guevara (1984), K-Ar determination of late Tertiary and Quaternary Andean volcanic rocks, southern Peru, *Geochem. J.*, *18*, 233–239.

Kennan, L. (2000), Large-scale geomorphology of the Andes: Interrelationships of tectonics, magmatism and climate, in *Geomorphology and Global Tectonics*, edited by M. A. Summerfield, pp. 167–199, John Wiley, Hoboken, N. J.

Kennan, L., S. Lamb, and C. Rundle (1995), K-Ar dates for the Altiplano and Cordillera Oriental of Bolivia: Implications for Cenozoic stratigraphy and tectonics, *J. S. Am. Earth Sci.*, *8*, 163–186.

Kirschvink, J. L. (1980), The least-square line and plane and the analysis of paleomagnetic data, *Geophys. J. R. Astron. Soc.*, *62*, 699–718.

Kley, J. (1999), Geologic and geometric constraints on a kinematic model of the Bolivian orocline, *J. S. Am. Earth Sci.*, *12*, 221–235.

Kley, J., and C. R. Monaldi (1998), Tectonic shortening and crustal thickness in the central Andes: How good is the correlation?, *Geology*, *26*, 723–726.

Kono, M., Y. Fukao, and A. Yamamoto (1989), Mountain building in the central Andes, *J. Geophys. Res.*, *94*, 3891–3905.

Lamb, S. (2001), Vertical axis rotation in the Bolivian orocline, South America: 1. Paleomagnetic analysis of Cretaceous and Cenozoic rocks, *J. Geophys. Res.*, *106*, 26,605–26,632.

Lamb, S., and L. Hoke (1997), Origin of the high plateau in the central Andes, Bolivia, South America, *Tectonics*, *16*, 623–649.

Lamb, S., L. Hoke, L. Kennan, and J. Dewey (1997), Cenozoic evolution of the central Andes in Bolivia and northern Chile, in *Orogeny Through Time*, edited by J.-P. Burg and M. Ford, *Geol. Soc. Spec. Publ.*, *121*, 237–264.

Latorre, O., Y. Orós, T. Sempere, M. Fornari, and V. Carlotto (2004), Estratigrafía y evolución paleógenas del área de Llalli-Macari (departamento de Puno), in *Nuevas contribuciones del IRD y sus contrapartes al conocimiento geológico del sur del Perú*, *Publ. Espec. 5*, edited by J. Jacay and T. Sempere, pp. 111–119, Soc. Geol. del Perú, Lima.

Luyendyk, B. P., M. J. Kamerling, R. R. Terres, and J. S. Hornafius (1985), Simple shear of southern California during Neogene time suggested by paleomagnetic declinations, *J. Geophys. Res.*, *90*, 12,454–12,466.

Lyon-Caen, H., P. Molnar, and G. Suárez (1985), Gravity anomalies and flexure of the Brazilian shield beneath the Bolivian Andes, *Earth Planet. Sci. Lett.*, *75*, 81–92.

Mamani, M., I. Ibarra, G. Carlier and M. Fornari (2004), Petrología y geoquímica del magmatismo alcalino de la zona noroeste del Altiplano peruano (departamento de Puno), in *Nuevas contribuciones del IRD y sus contrapartes al conocimiento geológico del sur del Perú*, *Publ. Espec. 5*, edited by J. Jacay and T. Sempere, pp. 157–174, Soc. Geol. del Perú, Lima.

Marshall, L., T. Sempere, and M. Gayet (1993), The Petaca (Late Oligocene–Middle Miocene) and Yecua (late Miocene) Formations of the Subandean–Chaco Basin, Bolivia, and their tectonic significance, *Doc. Lab. Geol. Lyon Fr.*, *125*, 291–301.

McFadden, P. L., and M. W. McElhinny (1988), The combined analysis of remagnetization circles and direct observations in paleomagnetism, *Earth Planet. Sci. Lett.*, *87*, 161–172.

McFadden, P. L., and M. W. McElhinny (1990), Classification of the reversal test in paleomagnetism, *Geophys. J. Int.*, *130*, 725–729.

McQuarrie, N. (2002), The kinematic history of the central Andean fold-thrust belt, Bolivia: Implications for building a high plateau, *Geol. Soc. Am. Bull.*, *114*, 950–963.

McQuarrie, N., and P. DeCelles (2001), Geometry and structural evolution of the central Andean backthrust belt, *Bolivia, Tectonics*, *20*, 669–692.

Müller, J. P., J. Kley, and V. Jacobshagen (2002), Structure and Cenozoic kinematics of the Eastern Cordillera, southern Bolivia (21°S), *Tectonics*, *21*(5), 1037, doi:10.1029/2001TC001340.

Newell, N. D. (1949), Geology of the lake Titicaca region, Peru and Bolivia, *Mem. Geol. Soc. Am.*, *36*, 111 pp.

Noble, D. C., and E. H. McKee (1977), Comment on spatial distribution of earthquakes and subduction of the Nazca plate beneath South America, *Geology*, *5*, 576–578.

Pardo-Casas, F., and P. Molnar (1987), Relative motion of the Nazca (Farallon) and South American plates since Late Cretaceous time, *Tectonics*, *6*, 233–248.

Randall, D. E. (1998), A new Jurassic-Recent apparent polar wander path for South America and a review of central Andean tectonic models, *Tectonophysics*, *299*, 49–74.

Randall, D. E., G. K. Taylor, and J. Grocott (1996), Major crustal rotations in the Andean margin: Paleomagnetic results from the Coastal Cordillera of northern Chile, *J. Geophys. Res.*, *101*, 15,783–15,798.

Randall, D. E., A. J. Tomlinson, and G. K. Taylor (2001), Paleomagnetically defined rotation from the Precordillera of northern Chile: Evidence of localized in situ fault-controlled rotations, *Tectonics*, *20*, 235–254.

Renne, P. R., C. C. Swisher, A. L. Deino, D. B. Karner, T. L. Owens, and D. J. DePaolo (1998), Intercalibration of standards, absolute ages and uncertainties in $^{40}Ar/^{39}Ar$ dating, *Chem. Geol.*, *145*, 117–152.

Richards, D. R., R. F. Butler, and T. Sempere (2004), Vertical-axis rotations determined from paleomagnetism of Mesozoic and Cenozoic strata of the Bolivian Andes, *J. Geophys. Res.*, *109*, B07104, doi:10.1029/2004JB002977.

Riller, U., and O. Oncken (2003), Growth of the central Andean Plateau by tectonic segmentation is controlled by the gradient in crustal shortening, *J. Geol.*, *111*, 367–384.

Rod, E. (1960), Geologic reconnaissance of Upper Ypacani River, Bolivia, *Am. Assoc. Pet. Geol. Bull.*, *44*, 1818–1828.

Rodríguez, R., T. Flores, and R. Marocco (1999), Análisis sedimentológico y estratigráfico de la Formación Tinajani (Cenozoico del Altiplano del Sur del Perú). Aportes a la reconstrucción de la evolución tectono-sedimentaria del Sur del Perú entre el Oligoceno superior y el Mioceno superior, *Bol. Soc. Geol. Peru*, *89*, 33–44.

Roperch, P., and G. Carlier (1992), Paleomagnetism of Mesozoic rocks from the central Andes of southern Peru: Importance of rotations in the development of the Bolivian Orocline, *J. Geophys. Res.*, *97*, 17,233–17,249.

Roperch, P., G. Hérail, and M. Fornari (1999), Magnetostratigraphy of the Miocene Corque basin, Bolivia: Implication for the geodynamic evolution of the Altiplano during the late Tertiary, *J. Geophys. Res.*, *104*, 20,415–20,429.

Roperch, P., M. Fornari, G. Hérail, and G. V. Parraguez (2000), Tectonic rotations within the Bolivian Altiplano: Implications for the geodynamic evolution of the central Andes during the late Tertiary, *J. Geophys. Res.*, *105*, 795–820.

Rousse, S. (2002), Apport du paléomagnétisme à l'étude des déformations lithosphériques au Pérou: Contraintes spatiales et temporelles sur la construction des Andes, Ph.D. thesis, 252 pp., Inst. de Phys. du Globe de Paris, Paris.

Rousse, S., S. Gilder, D. Farber, B. McNulty, P. Patriat, V. Torres, and T. Sempere (2003), Paleomagnetic tracking of mountain building in the Peruvian Andes since 10 Ma, *Tectonics*, *22*(5), 1048, doi:10.1029/2003TC001508.

Schmitz, M. A., W.-D. Heinsohn, and F. R. Schilling (1997), Seismic, gravity and petrological evidence for partial melt beneath the thickened central Andean crust (21–23°S), *Tectonophysics*, *270*, 313–316.

Sempere, T., G. Hérail, J. Oller, and M. Bonhomme (1990), Late Oligocene–early Miocene major tectonic crisis and related basin in Bolivia, *Geology*, *18*, 946–949.

Sempere, T., R. F. Butler, D. R. Richards, L. G. Marshall, W. Sharp, and C. C. Swisher III (1997), Stratigraphy and chronology of Upper Cretaceous-lower Paleogene strata in Bolivia and northwest Argentina, *Geol. Soc. Am. Bull.*, *109*, 709–727.

Sempere, T., G. Carlier, P. Soler, M. Fornari, V. Carlotto, J. Jacay, D. Néraudeau, J. Cárdenas, S. Rosas, and N. Jiménez (2002a), Late Permian-Middle Jurassic lithospheric thinning in Peru and Bolivia, and its bearing on Andean-age tectonics, *Tectonophysics*, *345*, 153–181.

Sempere, T., et al. (2002b) Lithospheric-scale transcurrent fault systems in the Andean southern Peru, paper presented at 5th International Symposium of Andean Geodynamics, Inst. de Rech. pour le Dév., Paris.

Sheffels, B. (1995), Is the bend in the Bolivian Andes an Orocline? in *Petroleum Basins of South America*, edited by A. J. Tankard, R. Suarez-Soruco, and H. J. Welsink, *AAPG Mem.*, *62*, 511–522.

Sigé, B., T. Sempere, R. F. Butler, L. G. Marshall, and J.-Y. Crochet (2004), Age and stratigraphic reassessment of the fossil-bearing Laguna Umayo red mudstone unit, SE Peru, from regional stratigraphy, fossil record, and paleomagnetism, *Geobios*, *37*, 771–794.

Somoza, R., and A. Tomlinson (2002), Paleomagnetism in the Precordillera of northern Chile (22°30′S): Implication for the history of tectonic rotations in the central Andes, *Earth Planet. Sci. Lett.*, *194*, 369–381.

Somoza, R., S. Singer, and B. Coira (1996), Paleomagnetism of upper Miocene ignimbrites at the Puna: An analysis of vertical-axis rotations in the central Andes, *J. Geophys. Res.*, *101*, 11,387–11,400.

Springer, M. (1999), Interpretation of heat-flow density in the central Andes, *Tectonophysics*, *306*, 377–395.

Steiger, R. H., and E. Jager (1978), Subcommission on Geochronology; convention on the use of decay constants in geochronology and cosmochronoly, in Contributions to the geologic time scale, edited by G. V. Cohee, M. F. Glaessner, and H. D. Hedberg, *Stud. Geol. Tulsa Okla.*, *6*, 67–71.

Swenson, J. L., S. L. Beck, and G. Zandt (2000), Crustal structure of the Altiplano from broadband regional waveform modeling: Implication for the composition of thick continental crust, *J. Geophys. Res.*, *105*, 607–621.

Tsunakawa, H., H. Tanaka, K. Amano, and M. Kono (1987), Paleomagnetic study of Late Miocene and early Pliocene rocks from southern Peru, central Andes, *J. Geomagn. Geoelectr.*, *39*, 477–486.

Victor, P., O. Oncken, and J. Glodny (2004), Uplift of the western Altiplano plateau: Evidence from the Precordillera between 20° and 21°S (northern Chile), *Tectonics*, *23*, TC4004, doi:10.1029/2003TC001519.

Vílchez, L. V., and A. H. Romero (1998), *Geología de los cuadrángulos de Río Pinquén, Pilcopata y Chontachaca. Hojas: 25–t, 26–t y 27–t*, 155 pp., Inst. Geol. Minero y Metalúrg., Lima.

Viramonte, J. G., S. M. Kay, R. Becchio, M. Escayola, and I. Novitski (1999), Cretaceous rift related magmatism in central-western South America, *J. S. Am. Earth Sci.*, *12*, 109–121.

Watson, G. S., and R. J. Enkin (1993), The fold test in paleomagnetism as a parameter estimation problem, *Geophys. Res. Lett.*, *20*, 2135–2137.

Wigger, P. J., et al. (1994), Variation in the crustal structure of the southern central Andes deduced from Seismic refraction investigations, in *Tectonics of the Southern central Andes: Structure and Evo-*

lution of an Active Continental Margin, edited by K. J. Reutter, E. Scheuber, and P. J. Wigger, pp. 23–48, Springer, New York.

Yang, Y., M. Liu, and S. Stein (2003), A 3-D geodynamic model of lateral crustal flow during Andean mountain building, *Geophys. Res. Lett.*, *30*(21), 2093, doi:10.1029/2003GL018308.

Yuan, X., et al. (2000), Subduction and collision processes in the central Andes constrained by converted seismic phases, *Nature*, *408*, 958–961.

Yuan, X., S. V. Sobolev, and R. Kind (2002), Moho topography in the central Andes and its geodynamic implications, *Earth Planet. Sci. Lett.*, *199*, 389–402.

M. Fornari, Institut de Recherche pour le Développement, UMR Géosciences Azur, Faculté des Sciences, F-06108 Nice Cedex 02, France.

S. Gilder, Institut de Physique du Globe de Paris, Laboratoire de Paléomagnétisme, 4 place Jussieu, F-75252 Paris Cedex 05, France. (gilder@ipgp.jussieu.fr)

S. Rousse, NGU, Geodynamic Laboratory, Leiv Eirikssons vei 39, N-7040 Trondheim, Norway.

T. Sempere, Institut de Recherche pour le Développement, Laboratoire Mécanismes de Transfert en Géologie, Institut des Sciences de la Terre, 14 avenue Edouard-Belin, F-31400 Toulouse, France.